GLIA

WILEY

## RESEARCH ARTICLE

# Human iPSC-derived endothelial cells promote CNS remyelination via BDNF and mTORC1 pathway

Dan Ma[1,2] | Huiyuan Zhang[1,3,4] | Le Yin[2,3,4] | Hao Xu[1,3,4] | Lida Wu[2,3,4] | Rahul Shaji[2] | Fatema Rezai[2] | Ayesha Mulla[2] | Sukhteerath Kaur[2] | Shengjiang Tan[5] | Boris Kysela[2] | Yilong Wang[6] | Zhiguo Chen[7] | Chao Zhao[1] | Yuchun Gu[2,3,4]

[1]Wellcome Trust-Medical Research Council Cambridge Stem Cell Institute and Department of Clinical Neurosciences, University of Cambridge, Cambridge, UK

[2]Translational Medicine Research Group (TMRG), Aston Medical School, Aston University, Birmingham, UK

[3]Molecular Pharmacology Laboratory, Institute of Molecular Medicine, Peking University, Beijing, China

[4]ALLIFE Medical Science and Technology Co. Ltd, Beijing, China

[5]Wellcome Trust-Medical Research Council Cambridge Stem Cell Institute and Department of Haematology, University of Cambridge, Cambridge, UK

[6]Department of Neurology, Tiantan Hospital Capital Medical University, National Center and National Clinical Research Center for Neurological Diseases, Advanced Innovation Center for Human Brain Protection, Chinese Institute for Brain Research, Beijing, China

[7]Cell Therapy Center, Beijing Institute of Geriatrics, Xuanwu Hospital Capital Medical University, National Clinical Research Center for Geriatric Diseases, and Key Laboratory of Neurodegenerative Diseases, Ministry of Education, Beijing, China

**Correspondence**
Dan Ma, Translational Medicine Research Group (TMRG), Aston Medical School, Aston University, Birmingham, UK.
Email: d.ma@aston.ac.uk

Chao Zhao, Wellcome Trust-Medical Research Council Cambridge Stem Cell Institute and Department of Clinical Neurosciences, University of Cambridge, Cambridge, CB2 0AH, UK.
Email: czhao@altoslabs.com

Yuchun Gu, ALLIFE Medical Science and Technology Co. Ltd, Beijing, China.
Email: guyuchun@allifetech.com

## Abstract

Damage of myelin is a component of many diseases in the central nervous system (CNS). The activation and maturation of the quiescent oligodendrocyte progenitor cells (OPCs) are the crucial cellular processes for CNS remyelination, which is influenced by neuroinflammation in the lesion microenvironment. Endothelial cells derived from human induced pluripotent stem cells (hiPSC-ECs) have shown promise in restoring function in various preclinical animal models. Here we ask whether and whether transplantation of hiPSC-ECs could benefit remyelination in a mouse model of CNS demyelination. Our results show that *in vitro*, hiPSC-ECs increase OPC proliferation, migration and differentiation via secreted soluble factors including brain-derived neurotrophic factor (BDNF). hiPSC-ECs also promote the survival of oligodendrocyte lineage cells *in vitro* and *in vivo*. Transplantation of hiPSC-ECs into a toxin-induced demyelination lesion in mouse corpus callosum (CC) leads to increased density of oligodendrocyte lineage cells and level of myelin in demyelinated area, correlated with a decreased neuroinflammation and an increased proportion of pro-regenerative M2 phenotype in microglia/macrophages. The hiPSC-EC-exposed oligo-dendrocyte lineage cells showed significant increase in the level of phosphorylated S6 ribosomal protein (pS6) both *in vitro* and *in vivo*, indicating an involvement of

Dan Ma and Huiyuan Zhang contributed equally to this work and share first authorship.

mTORC1 pathway. These results suggest that hiPSC-ECs may benefit myelin protection and regeneration which providing a potential source of cell therapy for a wide range of diseases and injuries associated with myelin damage.

**KEYWORDS**
BDNF, endothelial cell, iPSC, mTORC1, neuroinflammation, oligodendrocyte, remyelination

# 1 | INTRODUCTION

Damage of myelin is a component of many CNS diseases, these include multiple sclerosis (MS), traumatic injury, neurodegenerative diseases such as Alzheimer's disease, and mental disorders such as schizophrenia (Barateiro et al., 2016). Failure of remyelination eventually leads to progressive neuronal loss and irreversible functional deficits, therefore, promoting remyelination emerges as a potentially effective clinical intervention such as for progressive MS (Franklin & ffrench-Constant, 2017). Remyelination involves activation and recruitment of OPCs, the residential stem cells in CNS. They proliferate, migrate and differentiate into new mature oligodendrocytes and form new myelin sheaths (Crawford et al., 2013; Franklin & ffrench-Constant, 2017). Currently there is no treatment directly promoting remyelination in the clinic.

Progression of OPCs to mature myelinating oligodendrocytes involves complex interactions from several intrinsic signaling pathways, including the MAP kinase pathway, the mTOR pathway, and the Wnt signaling pathway. They are also modulated by an array of extrinsic factors (Adams et al., 2021). It has been known that the microvessels play crucial roles in myelin development and repair by providing vascular scaffold for OPC migration mediated by signaling molecules expressed from endothelial cells (Niu et al., 2019; Rajani et al., 2018; Tsai et al., 2016). Cerebral endothelial cells secrete trophic factors that support the survival and proliferation of OPCs, and this OPC-supportive phenomenon is mediated by Akt and Src signaling pathways (Arai & Lo, 2009).

Remyelination is orchestrated by multiple cell types in the microenvironment of demyelinated area (Baaklini et al., 2019). Upon demyelination, microglia/macrophages are activated, they remove myelin debris, secrete cytokines and growth factors which create a conducive environment for generation of oligodendrocytes from OPCs (Rawji et al., 2020). Inflammation plays an important role in remyelination. Remyelination involves an efficient proinflammatory M1 to anti-inflammatory M2 phenotype switch. Overreaction of inflammation or late switch is unbeneficial to the process (Franklin & Simons, 2022). Developing interventions which can effectively alter the physical and biological attributes in environment favoring new oligodendrocyte production presents a promising direction for clinical translation.

Human iPSC-ECs have been shown to be able to improve tissue restoration after ischemic damage in heart, limb and brain, either by direct cell replacement or by cell interaction (Jang et al., 2019; Nakagomi et al., 2009). Transplantation of iPSC-derived vascular endothelial cells improves white matter recovery from ischemic damage via increased number of oligodendrocyte lineage cells and

suppressed the inflammatory response (Xu et al., 2020, 2023). However, the effects of hiPSC-EC on oligodendrocyte lineage progression during CNS remyelination and the underlying mechanisms have not been sufficiently explored.

In the present study, we test the effects of exogenous hiPSC-ECs on remyelination in toxin-induced CNS demyelination mouse model. We first demonstrate an improved induction rate and efficiency of ECs differentiated from human iPSCs by minor modification of the known protocol. We then show that transplantation of hiPSC-ECs promotes myelin repair through soluble released factors such as BDNF, which facilitates oligodendrocyte linage progression mediated by mTORC1 signaling pathway. hiPSC-ECs also promote microglial M2 polarization. The results suggest that hiPSC-ECs may have therapeutic potential for the diseases and injuries related to myelin damage in CNS.

# 2 | MATERIALS AND METHODS

## 2.1 | Animals

Sprague–Dawley rats, wild-type C57BL/6 mice and NOD-SCID immunodeficient mice were purchased from Charles River (Margate, UK). SOX10-GFP reporter carrier line with C57BL/6 background was provided by Richardson lab from University College London. The animals were housed in pairs or groups under standard conditions on a 12-h light/dark cycle with constant access to food and water. The animals were randomly allocated to experimental groups. All animal studies were conducted under the Animals (Scientific Procedures) Act 1986 Amendment Regulations 2012 following ethical review by the University of Cambridge Animal Welfare and Ethical Review Body (AWERB).

Immunosuppression in C57BL/6 mice (including SOX10-GFP reporter carrier line) was induced by administration orally of cyclosporine A (210 mg/L, Sigma-Aldrich, 32425) in drinking water supplemented with sucralose at 1 mg/L from 1 day before demyelination lesioning till the animal being perfused at the end of the experiments.

## 2.2 | Generation of human iPSCs and the characterization

### 2.2.1 | Human neonatal dermal fibroblast culture

Cryopreserved human neonatal dermal fibroblasts (HDFn, Thermo-Fisher Scientific, C0045C) were thawed and immediately seeded into

culture flasks in complete culture medium DMEM (ThermoFisher Scientific, 10569010) supplemented with 10% foetal bovine serum (FBS, ThermoFisher Scientific, A4766801), 100 U/mL Penicillin and 100 μg/mL Streptomycin (ThermoFisher Scientific, 15140122). When the cells reached 80%–90% confluence they were detached by twice diluted Accutase (PromoCell, C-41310) and sub-cultured up to 3rd passage.

## 2.2.2 | Production of hiPSC by Epi5 episomal reprogramming

Reprogramming of the human neonatal dermal fibroblasts was performed by using Epi5™ Episomal reprogramming kit with Yamanaka factors + Lin28 (ThermoFisher Scientific, A15960) according to the protocol provided by manufacturer. In brief, reprogramming factors (Oct3/4, Sox2, Klf4, Lin28, and L-Myc) were delivered in episomal vectors with an oriP/EBNA-1 (Epstein–Barr nuclear antigen-1) backbone. Electroporation was performed at 1600 V in three pulses for 10 ms for $1 \times 10^6$ cells in 100 μL reaction system through the Neon electroporator (ThermoFisher Scientific, NEON1). The cells were then seeded at a density of $1 \times 10^5$ cells/cm$^2$ on plates that had been pre-coated with the Matrigel matrix (Corning, 356238) in fibroblast culture medium. At day 7 after reprogramming, the medium was changed to TeSR-E8 (Stemcell Technologies, 05940). Human iPSC colonies were mechanically picked by capillary under inverted microscope from days 17 to 25 and transferred to separate wells of a 24-well plate. Subsequent passaging was performed using Accutase. hiPSCs were maintained on tissue-culture plates that had been precoated with Matrigel in TeSR-E8 medium. The medium was changed daily, and they were passaged every 3–4 days for 8–10 passages before used for further EC differentiation.

## 2.2.3 | Alkaline phosphatase staining

Undifferentiated hiPSCs possess high expression level of alkaline phosphatases. To identify this characteristic, cultured hiPSCs were fixed by 4% paraformaldehyde (Merck, 158127) in 1xPBS and stained with NBT/BCIP (Merck, 72091) according to the manufacture's protocol. After 1-h incubation in dark, cells were washed twice with water to remove the background staining. They were then observed and imaged by Nikon T2 microscope.

## 2.2.4 | Immunostaining of undifferentiated hiPSCs

To characterize the clones by various iPSC markers, cultured hiPSCs were fixed by 4% paraformaldehyde in 1xPBS and immune-stained for TRA-1-60, or SSEA-4, or NANOG, or OCT4 antibodies at 4°C for overnight (for antibodies see Table 1). After a brief wash with 1xPBS, Alexa488 or 594 conjugated donkey anti-rabbit or anti-mouse secondary antibodies were used for a 2-h incubation at room temperature together with DAPI (Merck, D9542) nuclear staining. The cells were then observed and imaged by Nikon Ti-E microscope.

## 2.2.5 | Teratoma assay

Five to eight million of hiPSCs were harvested by Accutase digestion, washed with 1xPBS and re-suspended in 200 μL diluted (1:1) Matrigel solution. Cells were injected subcutaneously into NOD-SCID immuno-deficient mice. Teratomas were excised 8 weeks after the injection. The mice were fixed by 4% paraformaldehyde in 1xPBS, and the tissue were dissected out. After sectioning, slides containing various regions of teratomas were stained by H&E method (Abcam, ab245880). The sections were then observed and imaged by Nikon T2 microscope.

## 2.2.6 | Karyotype analysis

For karyotype analysis, iPSCs were treated with 20 μg/mL Colcemid (Merck, 234109-M) at 37°C for 30 min, detached by 0.125% Trypsin (ThermoFisher Scientific, 25200056) and then treated with 0.075 M KCl. The cells were stained with freshly prepared 4% Giemsa stain in Gurr buffer (ThermoFisher Scientific, B21172.18) and examined under Nikon Ti-E microscope. The karyotype was printed by assigning a number to each sister chromatid pair.

## 2.3 | Differentiation of hiPSC-ECs and the characterization

### 2.3.1 | Differentiation of hiPSC to EC

Human iPSCs generated by Epi5 reprogramming from human dermal fibroblasts were maintained in TeSR-E8 medium. The hiPSCs were then differentiated to ECs based on a 2D monolayer, serum-free culture according to the method of Patsch et al. (2015). To improve the induction efficiency and yielding, we modified the protocol in several steps, including an optimized cell seeding density, adding additional inductive factors Activin A (StemCell Technologies, 78001) and ALK inhibitor SB431542 (StemCell Technologies, 72232), and removing insulin in the whole differentiation progress (Lian et al., 2013). For details of modification, see Figure S1a. The endothelial differentiation procedure is summarized in Figure 2a. Briefly, Activin A was added into iPSC priming medium at a final concentration of 50 ng/mL on day 0, then it was withdrawn on day 1. Insulin was removed out from all medium in the whole differentiation progress (Lian et al., 2013). SB431542 was added into the induction medium at a final concentration of 10 μM from day 3, then it was removed after 1 day by fresh medium. On day 5, the cells were directly re-plated onto fibronectin (Corning, 356008) coated plates without MACS or FACS sorting, followed by a medium change on the next day for further differentiation. On

**TABLE 1** Antibody list.

| Antibody | Host | Resource | Dilution for IHC | Dilution for ICC | Cat# |
|---|---|---|---|---|---|
| Anti-APC (Ab-7) (CC-1) | Mouse | Millipore | 1:150 | 1:150 | OP80 |
| Anti-Arg1 | Goat | Santa Cruz, Dallas, TX | 1:200 | N/A | Sc-18355 |
| Anti-BDNF | Rabbit | Proteintech | 1:1000 | 1:1000 | 28205-1-AP |
| Anti-BDNF | Rabbit | Peprotech | For neutralization | | 500-P84 |
| Anti-CD11b | Rat | Biolegend | 1:200 | 1:200 | 201819 |
| Anti-CD11b | Mouse | Bio Rad | 1:100 | 1:100 | MCA275 |
| Anti-CD31 | Mouse | Abcam | 1:100 | 1:100 | ab9498 |
| Anti-CD31 | Rat | BD Biosciences | 1:200 | N/A | 557355 |
| Anti-CD34 | Mouse | abcam | N/A | 1:100 | ab54208 |
| Anti-GFP | Rabbit | Abcam | 1:1000 | 1:1000 | ab290 |
| Anti-human mitochondria | Mouse | Millipore | 1:100 | N/A | MAB1273 |
| Anti-Iba1 | Rabbit | Wako Osaka, Japan | 1:1000 | 1:1000 | 019-10741 |
| Anti-Iba1 | Goat | Abcam | 1:300 | 1:300 | Ab5076 |
| Anti-KDR | Rabbit | Abcam | N/A | 1:100 | ab2349 |
| Anti-Ki67 | Mouse | Abcam | 1:100 | 1;100 | ab16667 |
| Anti-MBP | Rat | AbD Serotec | 1:300 | 1:300 | MCA4095 |
| Anti-MOG | Rabbit | Abcam | 1:1000 | 1:1000 | Ab255266 |
| Anti-Nanog | Rabbit | Abcam | N/A | 1:100 | ab109250 |
| Anti-Neurofilaments 200 | Rabbit | Abcam | 1:1000 | N/A | ab8135 |
| Anti-O4 clone 81 | Mouse | Millipore | N/A | 1:100 | MAB345 |
| Anti-Oct4 | Rabbit | Abcam | N/A | 1:100 | ab19857 |
| Anti-Olig2 | Rabbit | Millipore | 1:1000 | 1:1000 | AB9610 |
| Anti-Olig2 | Mouse | Millipore | 1:100 | 1:100 | MABN50 |
| Anti-PDGFRa | Rabbit | BD Biosciences | 1:1000 | N/A | 558774 |
| Phospho-S6 Ribosomal Protein (Ser240/244) | Rabbit | Cell Signaling | 1:1000 | 1:1000 | #5364 |
| Anti-SSEA4 | Mouse | Abcam | N/A | 1:100 | ab16287 |
| Anti-TNFa | Rabbit | ThermoFisher Scientific | 1:1000 | 1:1000 | ARC3012 |
| Anti-TRA-1-60 | Mouse | Abcam | N/A | 1:100 | ab16288 |
| Anti-vWF | Rabbit | ThermoFisher Scientific | N/A | 1:1000 | BS-10048R |
| Anti-VE-Cadherin | Rabbit | Cell Signaling | N/A | 1:100 | 2158S |
| Hoechst 33258 | | Sigma-Aldrich | 1 μg/mL | 1 μg/mL | B2883 |
| Donkey anti-Mouse IgG (H + L) Alexa Fluor 488 | Donkey | Thermo Fisher Scientific | 1:500 | 1:500 | A-21202 |
| Donkey anti-Mouse IgG (H + L) Alexa Fluor 594 | Donkey | Thermo Fisher Scientific | 1:500 | 1:500 | A-21203 |
| Goat anti-Mouse IgG2b Alexa Fluor 594 | Goat | Thermo Fisher Scientific | 1:500 | 1:500 | A21105 |
| Donkey anti-Rabbit IgG (H + L) Alexa Fluor 488 | Donkey | Thermo Fisher Scientific | 1:500 | 1:500 | A-21206 |
| Donkey anti-Rabbit IgG (H + L) Alexa Fluor 568 | Donkey | Thermo Fisher Scientific | 1:500 | 1:500 | A-10042 |
| Donkey anti-Rabbit IgG (H + L) Alexa Fluor 647 | Donkey | Thermo Fisher Scientific | 1:500 | 1:500 | A-31573 |
| Donkey anti-Goat IgG (H + L) Alexa Fluor 488 | Donkey | Thermo Fisher Scientific | 1:500 | 1:500 | A-11055 |
| Donkey anti-Goat IgG (H + L) Alexa Fluor 647 | Donkey | Thermo Fisher Scientific | 1:500 | 1:500 | A-21447 |
| Donkey anti-Rat IgG (H + L) Alexa Fluor 488 | Donkey | Thermo Fisher Scientific | 1:500 | 1:500 | A-21208 |
| Donkey anti-Rat IgG (H + L) Alexa Fluor 594 | Donkey | Thermo Fisher Scientific | 1:500 | 1:500 | A-21209 |

day 8–9, the differentiated ECs were harvested, and they were detected by EC characteristic markers CD31, VE-Cadherin and Von Willebrand Factor (VWF). For antibodies see Table 1. The hiPSC-EC purity was measured by immunocytochemistry against these markers. The hiPSC-EC induction were repeated for five times. hESC-ECs were differentiated by the same modified protocol. The induced hiPSC-ECs were purified by MACS with CD31 Microbeads (Miltenyi Biotec, 130-091-935) according to the manufacture's

instruction, the hiPSC-ECs with more than 98% purity were obtained.

### 2.3.2 | hiPSC-derived EC culture

hiPSC-EC expansion and passages were carried out in Stem-pro34 medium (ThermoFisher Scientific, 10639-011) plus 50 ng/mL VEGFA (StemCell Technologies, 78073) directly on culture dishes. A proportion of the hiPSC-ECs were cryopreserved by 10% DMSO in their culture medium. For *in vitro* and *in vivo* experiments, the passages were restricted within three times both before and after cryopreservation. They were then recovered or/and maintained in EGM-2 medium (Lonza, CC-3124). They were detached by TrypLE™ Express Enzyme (1X) (ThermoFisher Scientific, 12604013) and the pellets were re-suspended by either EGM-2 medium for co-culture or 1xPBS for transplantation.

### 2.3.3 | GFP lentiviral vector transduction

After initial passage, a proportion of the hiPSC-ECs were transduced with lentivirus that carried GFP, to enable transplanted hiPSC-ECs to be traced *in vivo*. GFP-lentivirus were packaged in 293T cells with pLVX-AcGFP1-N1 Vector (Clontech, Takara Bio, 612354) and Lenti-X™ HT Packaging System (Clontech, Takara Bio, 632160 and 632161) according to manufacturer's protocol. Both GFP-transduced and non-transduced hiPSC-ECs were used for the following angiogenesis tests.

### 2.3.4 | Tube formation *in vitro*

The *in vitro* matrigel tube formation assay were performed according to Patsch et al. (2015). Briefly, the GFP positive hiPSC-ECs ($7 \times 10^4$) were plated on a 48-well plate coated with 300 μL Matrigel and cultured for 24 h in EGM-2 medium. The cells were then fixed by 4% paraformaldehyde for 10 min at room temperature, then they were observed by Zeiss inverted microscope (Axio Observer A1) either directly for GFP positive cells or after labeled for CD31 by immunocytochemistry. The hESC-ECs were also tested by the same protocol.

### 2.3.5 | Matrigel plug angiogenesis assay *in vivo*

To evaluate the ability of the hiPSC-ECs in angiogenesis *in vivo*, a mixture of 5 mg/mL Matrigel and hiPSC-ECs with a final density of 2000 cells/μL in ice-cold 1xPBS was injected subcutaneously into the flank of immunosuppressed C57BL/6 mice (6–8 weeks old, $n = 3$) at 200 μL per mouse. The negative controls contained Matrigel 1xPBS only. After 7 days, the mice were perfused by 4% paraformaldehyde; the Matrigel plugs were harvested, post-fixed and sectioned by cryostat (Bright Instruments, UK). The presence of capillaries in the Matrigel was detected by immuno-staining of GFP or CD31, the sections were observed with Zeiss inverted microscope (Axio Observer A1).

### 2.4 | Isolation and culture of rat oligodendrocyte progenitor cells and microglia

OPCs were isolated from neonatal Sprague Dawley rats at P2 to P3 by mechanical dissociation of mixed glial cultures as described (Chen et al., 2007; Mccarthy & de Vellis, 1980; Zhao et al., 2015). Microglia were removed by differential adhesion to uncoated plastic petri dishes. OPCs present in the supernatant were pelleted by centrifugation ($200 \times g_{max}$ for 5 min) and seeded on poly-d-lysine (PDL, Sigma, P6407) coated 24-well cell culture plates at a density of $3 \times 10^4$ per well in OPC medium [DMEM F-12 (ThermoFisher Scientific, 11320033) supplemented with 60 mg/mL N-acetyl cysteine (Sigma, P4333), 10 mg/mL human recombinant insulin (GIBCO, 12585), 1 mM sodium pyruvate (GIBCO, 11360070), 50 mg/mL apo-transferrin (Sigma, T2036), 16.1 mg/mL putrescine (Sigma, P5780), 40 ng/mL sodium selenite (Sigma, S5261), 60 ng/mL progesterone (Sigma, P8783), 330 mg/mL bovine serum albumin (Sigma, A4919), together with growth factors 10 ng/mL Recombinant Human PDGF-AA (PDGF-AA, Peprotech, 100-13A) and 10 ng/mL Recombinant Human FGF-basic (FGF2, Peprotech, 100-18B)] (Neumann et al., 2019). Cells were incubated at 37°C with 5% $CO_2$ and maintained using standard cell culture techniques. OPCs were maintained in the OPC medium with 4 days in growth factors before switching to differentiation medium, which is the OPC medium without growth factors but instead with thyroid hormone (T3, Sigma, T6397) at 40 ng/mL for 2–4 days. Cells were fixed with 4% paraformaldehyde before being analyzed for survival, proliferation, and differentiation by immunohistochemistry.

To obtain primary microglia, the rat mix glia from OPC preparation were used when they reached confluence (10–14 days). The flask was shaken at 150 rpm for 2 h and the floating cells in medium were centrifuged for collecting the microglia. The pelleted cells were either suspended and were re-seeded ($3 \times 10^4/cm^2$) in DMEM F12 containing 10% FBS and 1 mM of sodium pyruvate in a PDL pre-coated culture dish (Wu et al., 2020).

### 2.5 | Co-culture of hiPSC-ECs with OPCs and microglia

For OPC co-culture, $3 \times 10^4$ hiPSC-ECs were first seeded on each culture insert (24-well Millicell hanging cell culture insert, 0.4 μm, polyethylene terephthalate; Millipore) with EGM-2 medium (PromoCell, C-22111), which contains 2% FBS, and cultured for 2 days. It was then inserted into the OPC culture well with 40 μL EGM-2 medium, duplicated, when OPC were seeded with 360 μL OPC medium (with or without growth factors) for 4 or 6 days, or inserted when OPC was switched to differentiation condition (withdrawing growth factors and adding T3 at 40 ng/mL) for 2–4 days. In the control group, the empty insert with 40 μL EGM-2 medium was placed into the OPC well. The medium was changed at every other day. OPCs were fixed with 4% paraformaldehyde before being analyzed for proliferation and differentiation by immunostaining of different markers. OPCs were also co-cultured with either hESC-ECs or

human umbilical vein endothelial cells (HUVEC, Caltag-Medsystems, ZHC-2102) by the same protocol.

For microglia co-culture, the preparation of iPSC-EC inserts was the same as for OPCs. The insert was then inserted into the microglia culture well with 80 μL EGM-2 medium, duplicated, after microglia were seeded with 400 μL microglia medium in PDL pre-coated 24-well dish for 1 day. They were co-cultured for 1 day before exploring different factors for 24 h. The microglia were then fixed with 4% paraformaldehyde for immunocytochemical analysis.

## 2.6 | Migration assay

The transwell migration assay was adapted from the published protocols for rat OPCs (Abbott et al., 2006). Briefly, immediately after isolation, $3 \times 10^4$ OPCs in 200 μL of OPC medium with growth factors were seeded onto a 24-well Millicell hanging cell culture insert (8 μm polyethylene terephthalate; Millipore), which was placed in a 24-well culture plate containing 700 μL of OPC medium with growth factors with or without $1 \times 10^4$ hiPSC-ECs seeded in the wells 2 days ago, duplicated. The OPCs were incubated for 4 h, then fixed with 4% paraformaldehyde for 10 min. OPCs remaining on top of the transwell membrane were removed by swabbing, and the membrane was inversely mounted on slides. The OPCs were immuno-labeled by Olig2 antibody with co-stained by DAPI. Cells that had migrated to the underside of the membrane were imaged by Zeiss Inverted Microscope for 8–10 random fields/well and counted manually.

## 2.7 | Measurement of BDNF by ELISA

To determine the amount of BDNF secreted by hiPSC-ECs, enzyme linked immunosorbent assay (ELISA) against BDNF (Abcam, ab212166) was performed on hiPSC-EC mono-cultured medium supernatants, according to manufacturer's instructions in duplicates from three independent replicates. hiPSC-ECs were seeded at $1 \times 10^4$ cell/cm$^2$ in EGM-2 medium and cultured for 2 days. Data were normalized to their final cell densities.

## 2.8 | BDNF neutralization and inflammatory factor stimulation

To determine if BDNF was involved in hiPSC-EC-mediated OPC behavior, OPCs grown with hiPSC-ECs, or with equal amount of EGM-2 medium as control were cultured in the presence of neutralizing antibody. BDNF antibody (Rabbit IgG isotype, Peprotech, 500-P84) was added to cultures immediately after OPCs were seeded onto PDL coated wells and refreshed every other day at a concentration of 1 μg/mL when changing the OPC medium. Rabbit IgG (Peprotech, 500-P00) at a concentration of 1 μg/mL was used in the control groups with or without hiPSC-ECs. Cultures were fixed after 4 days (for OPC) or 6 days (for OL) with 4% paraformaldehyde for immunocytochemical analysis.

To determine if iPSC-ECs affect the inflammatory responses in OPCs and microglia, the co-cultures were stimulated with pro-inflammatory cytokine tumor necrosis factor α (TNFα, Recombinant rat TNFα, Peprotech, 400-14) for 24 h at 50 ng/mL, together with BDNF neutralization as above. In separated experiment, the microglia were also stimulated with anti-inflammatory cytokine IL-4 (Recombinant rat IL-4, Peprotech, 200-04) for 24 h at 100 ng/mL together with BDNF neutralization as above. The cells were fixed after 24 h with 4% paraformaldehyde for immunocytochemical analysis.

## 2.9 | Focal demyelination and hiPSC-EC transplantation in mouse corpus callosum (CC)

Both wild-type C57BL/6 mice and SOX10-GFP mice (male and female, aged 9–10 weeks) were randomly selected and used. Mouse demyelinating lesions were created in CC by direct injection of 1% lysolecithin (LPC, Sigma, L4129) (Crawford et al., 2016). Briefly, immunosuppressed mice were anesthetized with isoflurane supplemented with buprenorphine (0.03 mg/kg, s.c.), and mounted onto a stereotactic Stoelting frame. The CC was targeted for LPC and hiPSC-EC injection, with coordinates at 1 mm lateral and −0.4 mm rostral to Bregma point as reference. Two microliters of 1% LPC prepared in 1xPBS were injected at a depth of 1.2 mm below the brain surface at a constant flow rate (0.5 μL/min). At 2–3 days post lesioning (dpl), when the demyelination injury had been established, two microliters of hiPSC-ECs suspension in 1xPBS were injected at the density of $2.5 \times 10^5$ cells/μL using the same coordinates for LPC injection, the control group was injected with 2 μL 1xPBS.

At 6 dpl (4 days after hiPSC-EC transplantation), wild-type mice ($n = 6$ control and $n = 4$ hiPSC-EC) were fixed by 4% paraformaldehyde for immunocytochemical analysis and FluoroMyelin (ThermoFisher Scientific, F34652) staining. At 11 dpl (8 days after hiPSC-EC transplantation), SOX10-GFP mice ($n = 7$ control and $n = 7$ hiPSC-EC) were fixed by 4% paraformaldehyde for immunocytochemical analysis. At 21 dpl (19 days after transplantation), wild-type mice ($n = 4$ control and $n = 5$ hiPSC-EC) were fixed by 4% glutaraldehyde (ThermoFisher, A10500.22) in 1xPBS for electron microscopy (EM) observation of remyelination. Also at 21 dpl, wild-type mice ($n = 3$) with hiPSC-EC transplantation were fixed by 4% paraformaldehyde for tracing the transplanted hiPSC-ECs.

## 2.10 | Tissue processing, immunofluorescence, and imaging

For histological observation, mice were terminally anesthetized with pentobarbitone and perfused through the left ventricle with 4% paraformaldehyde in 1xPBS, pH 7.4. The fixed brains containing the lesion were dissected, post-fixed in 4% paraformaldehyde overnight at 4°C, then immersed in 20% sucrose (Merck, S9378) in 1xPBS for 48 h

before embedding with optimal cutting temperature compound (Bright Instruments UK). Coronal frozen sections at a thickness of 12 μm were thaw mounted onto poly-L-lysine-coated slides (VWR, 631-0107) and stored at −80°C until further use.

Frozen sections, or fixed cultured cells, were rinsed in 1xPBS, then permeabilized and blocked with the blocking solution, containing 0.1% (v/v) Triton X-100 and 5% (v/v) normal donkey serum (Sigma, D9663) in 1xPBS for 1 h at room temperature (RT). The samples were then incubated for 12–16 h at 4°C with primary antibodies followed by incubation with fluorophore-conjugated secondary antibodies for 2 h at RT. Both primary and secondary antibodies were diluted in the blocking solution. For double labelling, a mixture of primary antibodies from different animal species and corresponding secondary antibodies conjugated with distinct fluorophore were used. The details for primary and secondary antibodies used this study are listed in Table 1. Cell nuclei were counterstained with DNA fluorescent dye DAPI. Demyelination lesion was defined by the cellularity through DAPI staining in CC. For myelin composition measurement, some sections were also incubated in FluoroMyelin in accordance with the kit protocol for myelin staining. Slides were then mounted in mounting media (Vectashield, H-1500).

The images for the stained samples were acquired using Zeiss Axio Observer A1 fluorescence microscope or Nikon Ti-E live cell imaging system. As indicated below, quantifications were performed either by eye or using high-content imaging and quantification, where appropriate.

## 2.11 | Electron microscopy analysis

For EM observation, mice were perfused at 21 dpl through the left ventricle with 4% glutaraldehyde in 1xPBS containing 0.4 mm CaCl$_2$, pH 7.4. The CCs were sliced in sagittal orientation at ~1 mm thickness and treated with 1% osmium tetroxide (Sigma 201030) overnight before going through epoxy resin embedding process described previously (Zhao et al., 2008). Lesion tissues were located on semithin (1 μm) sections stained with toluidine blue O (Merck, 198161). Ultrathin sections of the lesion site were cut onto copper grids and stained with uranyl acetate and lead citrate before image acquisition on Hitachi HT7800 Transmission EM. G-ratio was quantified on images with 3000× magnification on a minimum of 70 myelinated and remyelinated axons per animal, 3–5 mice for each group.

## 2.12 | TUNEL assay

TUNEL staining was performed on the cultured OPCs or on the brain sections from SOX10-GFP mice with CC lesion and hiPSC-EC transplantation, using the Click-iT™ Plus TUNEL Assay for in situ apoptosis detection with Alexa Fluor™ dyes 594 (ThermoFisher, C10618) according to the manufacturer's instructions. The Nikon Ti-E microscope was used for observation and image acquisition.

## 2.13 | Measurement and quantification

Image data were recorded as common formats such as Tiff or JPEG. Cell counting or measurement was obtained randomly from at least three areas (each well) for the cultured cells or three lesion areas throughout the entire lesion with minimum 0.2 mm intervals across the center of lesion site from individual mouse. For cell counting in lesion, the fluorescence-labeled cells were manually counted from the images captured under the same exposure conditions. The cell density was then obtained based on the lesion area measured by Zeiss Axivision or Nikon NIS software. Immunoreactive cells were counted only if they were clearly associated with DAPI stained nuclei. For measuring immunostaining intensity, the labeled cells or area were corrected with background then measured by using ImageJ software (Fiji) to get mean value for the fluorescence intensity (Fiji Intensity). For the labeling intensity in cells and in lesion, at least 10 objectives were randomly captured in each culture field (3× per well) or each lesion area (3× per mouse), then the average intensity of single cell was obtained. For immunolabeling intensities in CC lesion area, the whole lesion area (3× per mouse) was measured, and the average intensity was obtained for each mouse. Fiji software was also used for measuring the area density of immuno-labeled structure in lesion area; it was also used for measuring the length of OL branches. For quantifying oligodendrocyte morphology in culture, MBP+ processes >50 microns were considered as long processes. The images of samples were coded blinded to assessors.

## 2.14 | Statistical analysis

Statistical analysis was performed using GraphPad Prism8. Data were tested for normality of residuals (Kolmogorov–Smirnov test) and homogeneity of variance (Levene's test). Datasets passing both criteria were compared by either unpaired Student's $t$ test (if 2 groups), or one-way ANOVA with Tukey honest significant difference (HSD) post hoc tests (if >2 groups). Nonparametric data were compared by Mann–Whitney $U$ test (2 groups) or Kruskal−Wallis test with Dunn's post hoc test (>2 groups).

## 3 | RESULTS

## 3.1 | Generation of human iPSCs and efficient induction of endothelial cells

Human iPSCs were generated from human neonatal dermal fibroblasts by Yamanaka factors (OSKM) (Takahashi et al., 2007) using a commercially available Epi5 reprogramming Kit. The iPSCs possessed high expression level of alkaline phosphatases, showing undifferentiated status (Figure 1a). The iPSCs were also characterized and showed to be positive for the pluripotent markers OCT-4, NANOG, TRA-1-60 and SSEA-4 (Figure 1b). The iPSCs could develop into teratomas *in vivo*, and H&E staining showed three tissue types from
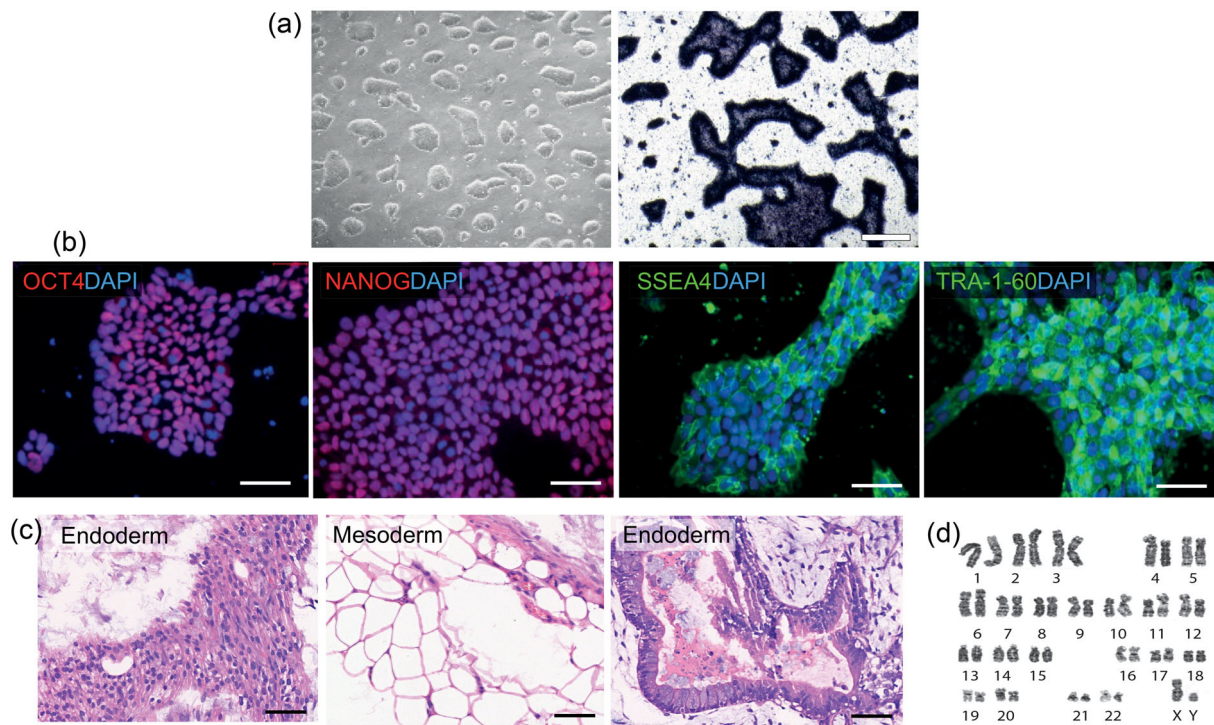
**FIGURE 1** Generation of induced human pluripotent stem cells (hiPSCs) and characterization. (a) The morphology of the hiPSC clones and their high expression of alkaline phosphatases, showing undifferentiated status. Scale bars, 200 μm. (b) Expression of the pluripotent markers OCT4, NANOG, SSEA-4, and TRA-1-60 in the hiPSC clones. Scale bars, 50 μm. (c) The hiPSCs developed into teratomas in NOD-SCID immunodeficient mice. H&E staining shows three tissue types including ectoderm (neural tissue/tube), mesoderm (adipose tissue), and endoderm (gastrointestinal tract). Scale bars, 50 μm. (d) The hiPSCs showed a normal human cell karyotype (46, XY) after 10 passages.

endoderm, mesoderm, and ectoderm (Figure 1c). The iPSCs also possessed normal karyotype (Figure 1d).

We then generated ECs from these the iPSCs using an established induction protocol (Patsch et al., 2015), with modifications (see Figure S1a) including an optimized cell seeding density, adding additional inductive factors Activin A and ALK inhibitor SB431542, and removing insulin in the whole differentiation progress (Lian et al., 2013). We consistently obtained ECs via an endothelial progenitor cell (EPC) stage (schematic illustration as in Figure 2a). We generated the iPSC-ECs with approximately 98% (98.0% ± 1.8%, *p* < .001) of the cells expressing characteristic EC markers CD31, Von Willebrand Factor (VWF) and VE-Cadherin (Figure 2c,d,f). The modified method showed an improved iPSC-EC yield indicating a higher efficiency compared to the original method (Figure 2e). We also induced ECs from H1 human ES cell line (hESC-EC) by using the same modified protocol, which showed similar results (Figure S1b, S1c). The generated hiPSC-ECs were harvested, and they were purified by magnetic-activated sorting (MACS) at the end of induction schedule before further *in vitro* and *in vivo* experiments.

To verify the angiogenesis capability of the induced hiPSC-ECs, we conducted angiogenesis assays both *in vitro* and *in vivo*. The iPSC-ECs manifested typical morphology of 'tube formation' on Matrigel coated dish surface (Figure 2g), and invasion of angiogenic sprouts post hoc into the Matrigel plug injected subcutaneously in mouse (Figure 2h). These tests confirmed the EC functional properties of the

hiPSC-ECs induced by the modified method. The hESC-ECs also showed tube formation *in vitro* (Figure S1d).

## 3.2 | hiPSC-ECs directly promote OPC proliferation, migration and differentiation by secreted factors

To assess the effects of hiPSC-ECs on OPC proliferation and differentiation, we co-cultured hiPSC-ECs with rat OPCs in transwell insert system, where the rat OPCs were seeded in the bottom of the wells and the hiPSC-ECs were plated on the membrane in the hanging inserts.

### 3.2.1 | hiPSC-ECs increase OPC proliferation, migration and differentiation

After co-cultured with hiPSC-ECs in OPC medium (with PDGF-AA and FGF2) for 4 days, there was a significant increase in OPC proliferation, as detected by a higher proportion of Ki67+ OPCs in total Olig2+ cells (11.60% control vs. 16.81% hiPSC-EC. *p* < .05), and an increased density of Olig2+ cells (109.40/field control vs. 178.20/field hiPSC-EC *p* < .05) (Figure 3a). OPC migration was tested with transwell insert system, in the presence of hiPSC-ECs, there was a significant increase in the number of OPCs migrated to the underside of the membrane through the
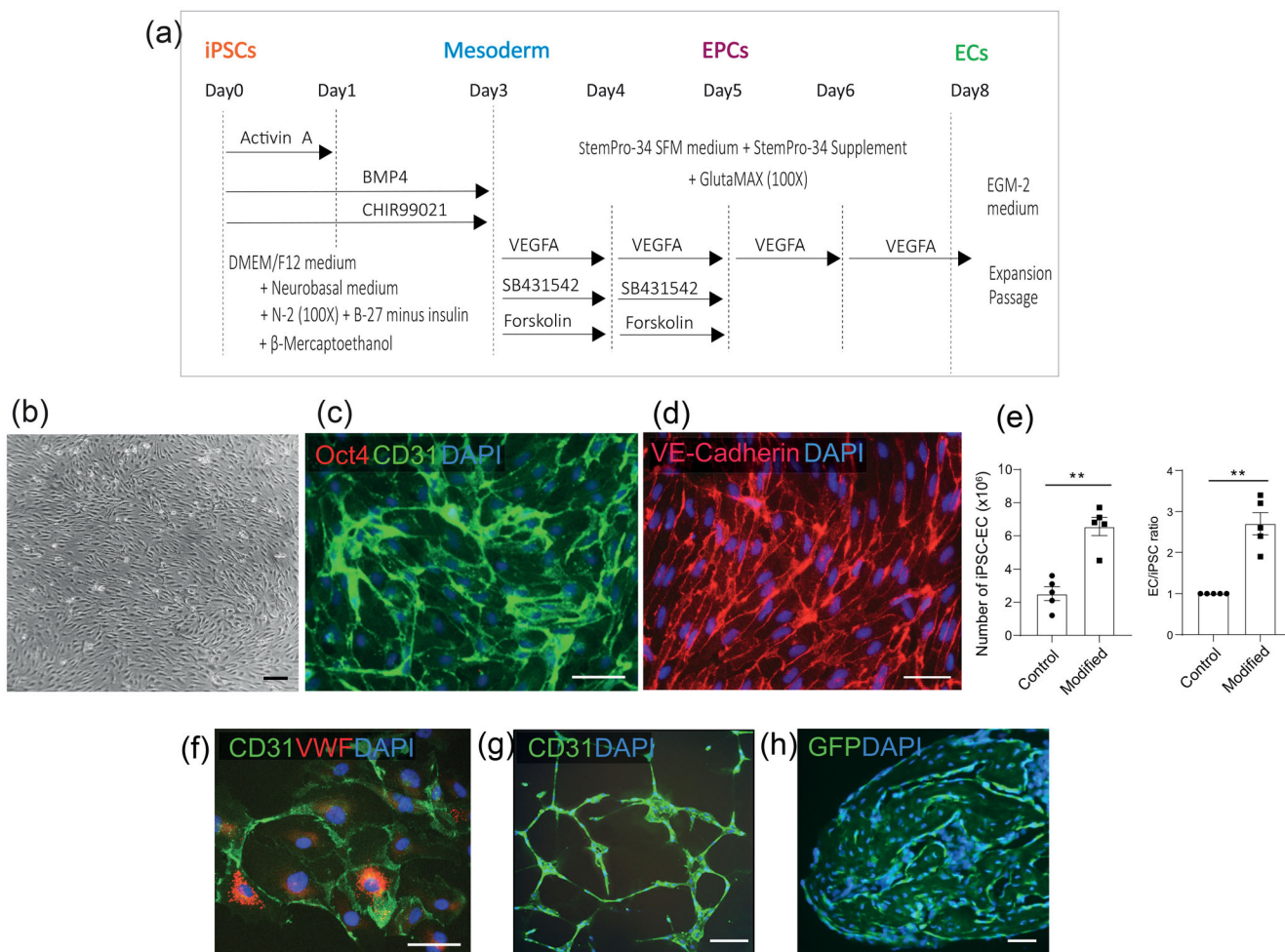
**FIGURE 2** Generation of human iPSCs-derived endothelial cells (hiPSC-ECs). (a) Schematic illustration of the procedure of EC differentiation from human iPSCs. The method was based on Patsch et al. (2015) with minor modifications (see Supplementary Figure S1). (b) Bright field image showing the morphology of hiPSC-ECs. Scale bars, 200 μm. (c) Representative image of induced hiPSC-ECs, which produced characteristic EC markers CD31 (green) but lost iPSC marker Oct4. Scale bar, 50 μm. (d) Representative image of the induced hiPSC-ECs, which produced characteristic EC marker VE-Cadherin. Scale bar, 50 μm. (e) Comparison of modified and original protocols on hiPSC-EC yield and induction efficiency at day 9, showing the improvements on both parameters. All data are presented as mean ± SE, $n = 5$, **$p < .01$. Unpaired $t$ test. (f) Representative image of induced hiPSC-ECs which expressed characteristic EC markers CD31 and vWF. Scale bar, 50 μm. (g) Angiogenesis test *in vitro*, showing Matrigel tube forming by hiPSC-ECs after 24 h culture which were labeled with CD31. Scale bar, 100 μm. (h) Angiogenesis test by Matrigel plug assay *in vivo*, showing the tube forming by GFP expressing hiPSC-ECs in matrigel plug after 7 days growing subcutaneously. Scale bar, 50 μm.

pores (7.4% control vs. 11.3% hiPSC-EC. $p < .05$. Figure 3b). Differentiation was assessed by switching to differentiation medium (withdrawal of PDGF-AA and FGF2, adding T3) in the co-culture system, and continue to grow with hiPSC-ECs for 2 days. There was a significant increase in the total number of differentiated OPCs, as labeled by the mature oligodendrocyte marker myelin basic protein (MBP) (38.52/field control vs. 88.48/field hiPSC-EC $p < .05$), and the percentage of MBP+ Olig2+ cells in total Olig2+ oligodendrocytes (10.39% control vs. 16.22% hiPSC-EC, $p < .05$) (Figure 3c). There was also an increase in the proportion of the MBP+ Olig2+ oligodendrocytes which had longer processes (12.2% control vs. 53.6% hiPSC-EC, $p < .01$. Figure 3d). These results indicate that the factors released from hiPSC-ECs promote oligodendrocyte lineage progression *in vitro*. We also co-cultured the

OPCs with hESC-ECs and HUVECs, the effects were similar as hiPSC-ECs exerted on OPC proliferation and differentiation (Figure S2a, S2b).

## 3.2.2 | hiPSC-ECs promote oligodendrocyte linage progression via secreted soluble factors including BDNF via mTORC1 pathway

BDNF is a neurotrophin that has been proven to promote CNS myelination during development and to enhance remyelination following myelin injury (Fletcher et al., 2018). Endothelial cells secrete trophic factors such as FGF and BDNF, which activate TrKB/Akt and mTORC1 signaling pathway, to sustain
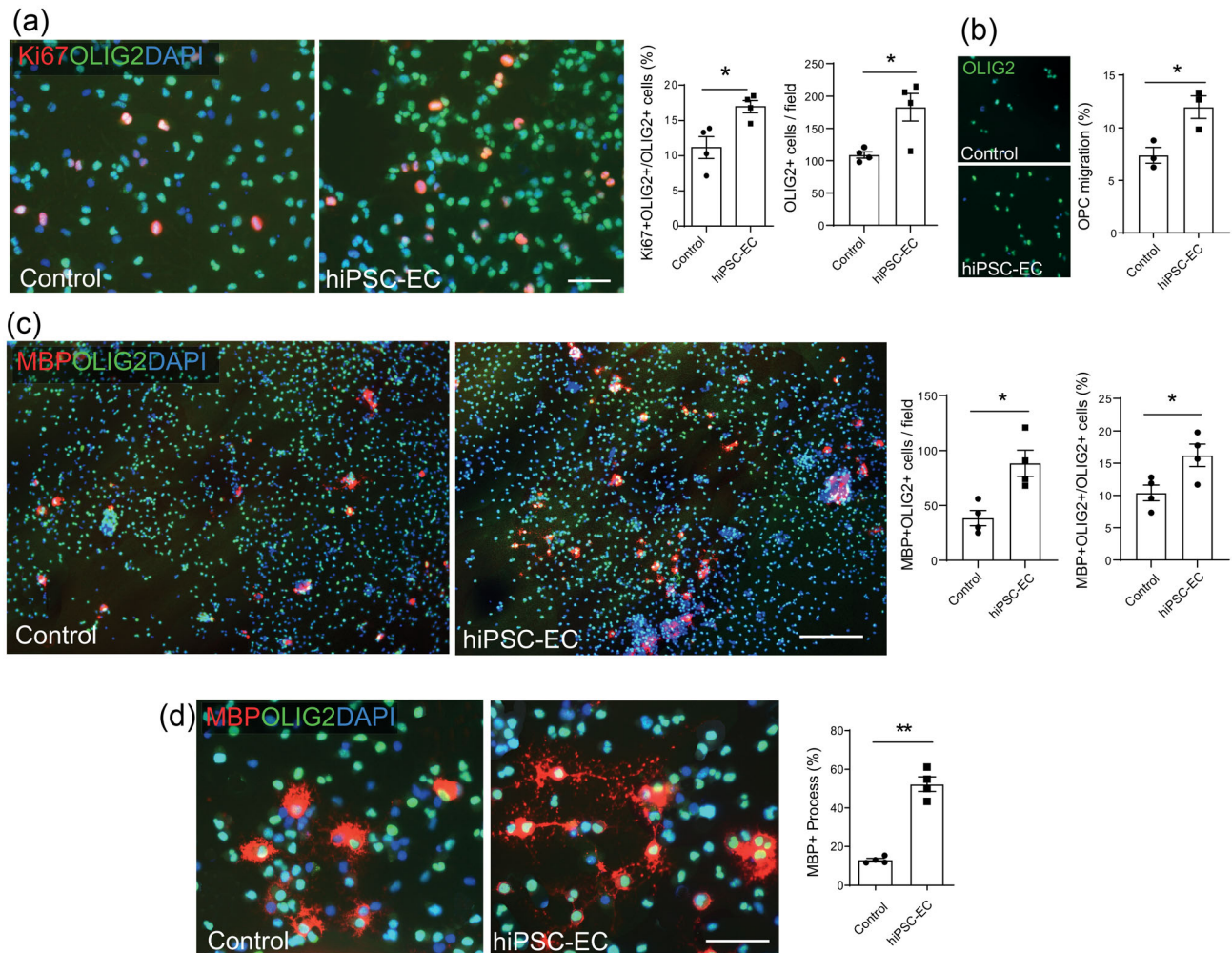
**FIGURE 3** Human iPSC-derived endothelial cells (hiPSC-ECs) enhance oligodendrocyte lineage progression *in vitro*. (a) Representative images of rat OPCs co-cultured with hiPSC-ECs in the transwell system in OPC medium. Immunostaining of Ki67 and Olig2 shows an increased OPC proliferation. Quantification shows a higher percentage of Ki67+ cells in total Olig2+ cells, and a higher total density of Olig2+ cells versus control. Scale bar, 50 μm. All data are presented as mean ± SE, $n = 4$, *$p < .05$. Unpaired *t* test. (b) Representative images of migrated OPCs (Olig2+) through membrane of transwell, and the quantification of the percentage of the migrated OPCs over total seeded OPCs, showing an increased OPC migration in the presence of hiPSC-ECs. Scale bar, 100 μm. All data are presented as mean ± SE, $n = 3$, *$p < .05$. Unpaired *t* test. (c) Representative images of the differentiated rat oligodendrocytes (MBP+) in the hiPSC-EC co-culture system in differentiation condition for 2 days. The quantification shows a significant increased cell density of MBP+ oligodendrocytes and an increased percentage of them in total Olig2+ cells. Scale bar, 200 μm. All data are presented as mean ± SE, $n = 4$, *$p < .05$. Unpaired *t* test. (d) Representative images of the rat MBP+ cells in hiPSC-EC co-culture system showing differentiated oligodendrocytes with long branches in the presence of hiPSC-ECs. The quantification shows an increased percentage of the MBP+ cells with long branches in the presence of hiPSC-ECs. All data are presented as mean ± SE, $n = 4$. *$p < .05$. Unpaired *t* test. Scale bar, 50 μm.

OPCs proliferation, survival and differentiation (Arai & Lo, 2009; Lebrun-Julien et al., 2014; Xiao et al., 2010). We examined the BDNF secretion from the hiPSC-ECs and the effects of its neutralization on OPC proliferation and differentiation. There was a strong BDNF labelling in hiPSC-ECs by immunocytochemistry (Figure 4a), with an intensity 1.8 folds higher than that in neuroblastoma SH-SY5Y cells ($p < .01$, data not shown). SH-SY5Y cells were used as control because they express low level of BDNF comparing with that of the differentiated neurons (Attoff et al., 2020). The level of the secreted BDNF in the hiPSC-EC culture medium were measured by ELISA, it reached 9.14 pg/mL/$10^6$ cells after 2 days culture, which was significantly

higher than that in EGM-2 medium (0.15 pg/mL/$10^6$ cells, $p < .001$. Figure 4b).

To examine whether the effects of hiPSC-ECs on OPCs were mediated by secreted BDNF, we tested OPCs co-cultured with hiPSC-ECs in the presence of BDNF neutralizing antibody. To minimize the compensatory effects from exogenous PDGF-AA and FGF2 when assessing the hiPSC-EC derived factors in this experiment, PDGF-AA and FGF2 were excluded from the OPC medium. This caused a significant reduction in OPC proliferation, detected by a lower proportion of Ki67+ OPCs in Olig2+ cells (24.05% with PDGF-AA/FGF2 vs. 15.87% without, $p < .05$), and a reduction in total OPC number (100.25 vs. 78.00 cells/field, $p < .05$)
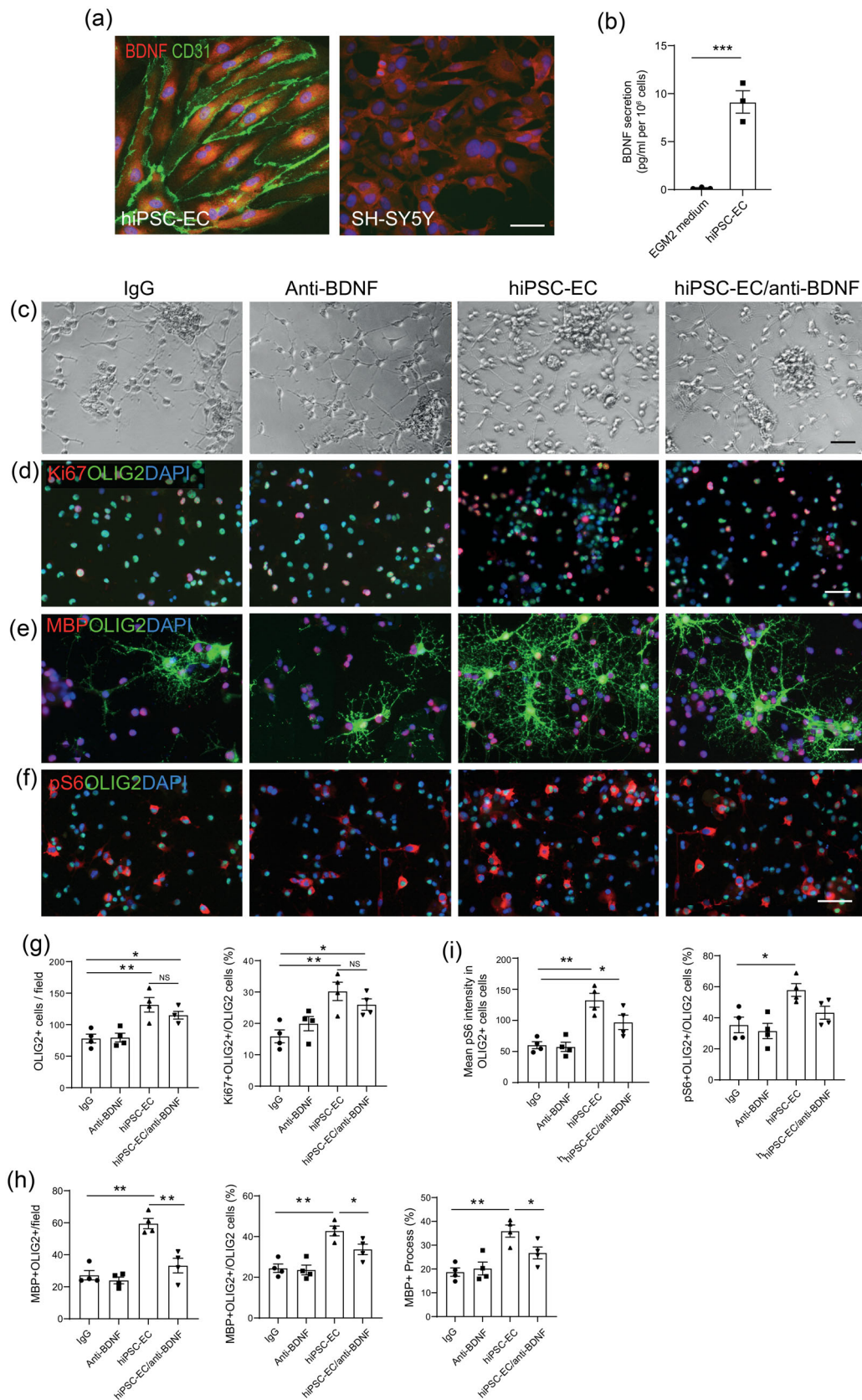
FIGURE 4    Legend on next page.

(Figure S2c), after 4 days in culture. However, in the presence of hiPSC-ECs, the OPCs showed a marked increase in proliferation, revealed by a higher density of Olig2+ cells (81.00/field control vs. 125.20/field hiPSC-EC, *p* < .05), as well as a higher proportion of ki67+ cells among them (16.84% control vs. 30.00% hiPSC-EC, *p* < .05) (Figure 4c,d,g). Moreover, 6 days after co-culture, there were more MBP+ Olig2+ oligodendrocytes (27.3/field control vs. 59.5/field hiPSC-EC, *p* < .01) and a higher proportion of MBP+ Olig2+ cells among Olig2+ oligodendrocyte lineage cells (24.4% control vs. 42.8% hiPSC-EC, *p* < .01. Figure 4e,h). Although there was no added T3, the 10% of EGM-2 medium supplement brought to a final 0.2% FBS in the OPC medium. Again, there were more MBP+ Olig2+ oligodendrocytes with longer processes (18.68% IgG control vs. 35.90% hiPSC-EC, *p* < .01. Figure 4e,h). The BDNF neuralisation did not altered the effect on proliferation (Figure 4d,g), but reduced the OPC differentiation, represented as a lower number of MBP+ Olig2+ cells, a decreased proportion of MBP+ Olig2+ cells, together with shorter processes (*p* < .01, *p* < .05, Figure 4e,h). These results indicate that hiPSC-ECs secrete multiple soluble factors that facilitate OPC proliferation and differentiation; among them BDNF could be partially attributed to the pro-differentiation effects on OPCs.

BDNF signaling is known to be involved in the activation of mTORC1 pathway which is crucial for oligodendrocyte differentiation (Adams et al., 2021; Lebrun-Julien et al., 2014; Xiao et al., 2010). To elucidate whether the effect of the secreted BDNF on OPC differentiation was associated with mTORC1 pathway, we also examined the level of phosphorylated forms of the downstream target pS6 (Ser240/244) in the OPCs co-cultured with hiPSC-ECs and BNDF antibody. The average intensity of pS6 labelling was much higher in the OPCs exposed to hiPSC-ECs (60.18 control vs. 135.56 hiPSC-EC, Fiji Intensity, *p* < .01. Figure 4f,i), together with a higher proportion of pS6+ cells in Olig2+ cells (35.4% control vs. 57.9% hiPSC-EC, *p* < .05. Figure 4f,i). However, the presence of BDNF neutralizing antibody did not revert these increases (Figure 4f,i), indicating that other factors secreted from

hiPSC-ECs also contributed to mTORC1 pathway activation and OPC differentiation.

### 3.2.3 | iPSC-ECs improve OPC survival after pro-inflammatory stimulation

Overreaction of neuroinflammation cause increased level of pro-inflammatory mediators such as TNFα which is mainly secreted from activated microglia (M1), this may lead to neuronal and glial cell damage (Lyman et al., 2014). Although TNFα stimulates OPC activation *in vivo* (Franklin & Simons, 2022), it promotes oligodendrocyte death and inhibits OPC differentiation *in vitro* (Bonora et al., 2014). To assess the effect of hiPSC-ECs on attenuating the damage caused by such pro-inflammatory factors in OPCs, and a potential protection from EC derived factors such as BDNF, we treated the OPCs with TNFα in the co-culture system. Our results showed that TNFα led to a higher percentage of TUNEL labelling (10.49% control vs. 19.34% TNFα, *p* < .01. Figure 5) and a reduced OPC density (81.00/field control vs. 45.67/field TNFα, *p* < .01). hiPSC-ECs partially reversed the change on the percentages (19.34% TNFα vs. 11.61% TNFα+ hiPSC-ECs, *p* < .05), which was blocked by anti-BDNF antibody (11.61% TNFα+ hiPSC-ECs vs. 20.31% TNFα+ hiPSC-ECs+ aBDNF, *p* < .05, Figure 5). These data indicate that hiPSC-ECs exhibit a protective effect on OPCs against pro-inflammatory stimulation, which involves their secreted BDNF.

### 3.3 | hiPSC-EC transplantation enhances myelin repair in toxin-induced demyelination model

Next, we tested the effects of transplantation of hiPSC-ECs on lysolecithin (LPC)-induced demyelination and remyelination in CC of mice. We examined the early (6 days post lesion, dpl), middle (11 dpl) and late (21 dpl) stages to assess myelin protection, OPC processing and myelin repair. The schematic illustration of the experiment is shown in Figure 6a. At 11 dpl, we also used the mice with GFP reporter expression controlled by SOX10 promoter for visualization

**FIGURE 4** Involvement of brain derived neurotrophic factor (BDNF) and mTORC1 activation in hiPSC-EC mediated effects on OPCs. (a) Representative images of hiPSC-ECs and SH-SY5Y cells with immunostaining of BDNF show an intensive labelling in hiPSC-ECs, compared to a relatively low expression in SH-SY5Y cells. Scale bar, 50 μm. (b) Release of BDNF by hiPSC-ECs evaluated by ELISA, the concentration of BDNF is significantly higher in hiPSC-EC culture supernatant than that in EGM-2 medium. Data are presented as mean ± SE, *n* = 3. ***p* < .001. Unpaired *t* test. (c) Representative set of bright field images of the OPCs in the presence of control IgG, or anti-BDNF antibody, or hiPSC-ECs plus IgG or hiPSC-EC plus anti-BDNF antibody for 4 days. Scale bar, 50 μm. (d) Immunocytochemical assessment of OPC proliferation with Ki67 and Olig2 co-labelling in cultures under the same conditions as in (c). As shown in quantification (g), hiPSC-ECs increased the total Olig2+ cell number per field and the percentage of Ki67+ OPCs in Olig2+ cells, while the neutralizing anti-BDNF antibody did not altered the effects. Scale bar, 50 μm. (e) Immunocytochemical assessment of OPC differentiation with MBP labelling in Olig2+ cells under the same conditions as in (c), but for 6 days. As shown in quantification (h), hiPSC-ECs increased the total MBP+ cell number per field and the percentage of MBP+ cells in Olig2+ cells, neutralizing anti-BDNF antibody partially reduced the enhancing effect. Scale bar, 40 μm. (f) Immunocytochemistry shows the pS6 labelling in Olig2+ cells in the conditions as in (c). As shown in quantification (i), the intensity of pS6 labelling and the percentage of pS6+ cells in total oligodendrocyte linage cells (Olig2+) were both increased in the presence of hiPSC-ECs, neutralizing anti-BDNF antibody did not attenuate the effect. Scale bar, 50 μm. (g) Quantification of (d), Ki67 and Olig2 labelling. (h) Quantification of (e), MBP and Olig2 labelling. (i) Quantification of (f), pS6 and Olig2 labelling. All data are presented as mean ± SE, *n* = 4, ***p* < .01, **p* < .05. One-way ANOVA with post hoc analysis.
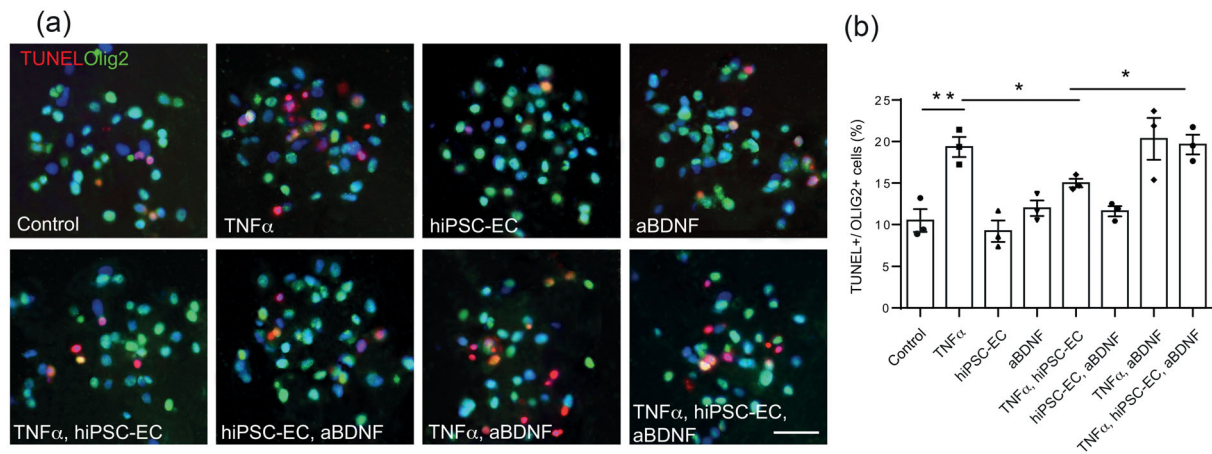
**FIGURE 5** hiPSC-ECs promote OPC survival against pro-inflammatory stimulation. (a) Representative images of TUNEL labeled OPCs treated with TNFα, hiPSC-ECs and anti-BDNF antibody. (b) Quantifications of (a) on proportion of TUNEL+ OPCs in total OPCs (here Olig2+). Scale bar, 30 μm. All data are presented as mean ± SE, $n = 4$, *$p < .05$. One-way ANOVA with post hoc analysis.

of oligodendrocyte lineage cells. Demyelination lesion was identified by a sharp increase of cellularity as shown by an aggregation of DAPI labeled nuclei in the CC area (Figure 6c).

### 3.3.1 | Survival and migration of the transplanted hiPSC-ECs

Double immunohistochemical staining for human specific antibodies against mitochondria together with antibody against endothelial cell markers (vWF) showed that the transplanted iPSC-ECs survived and maintained EC characteristics after 21 dpl (Figure 6b). The transplanted iPSC-ECs were not only aggregated at the graft site but also migrated into CC lesion area, either closely or overlapped to the lesion hence close to the recruited OPCs (Figure 6c). They also migrated to the nearby area into cortex and along the dorsal edge of CC from 6 to 21 dpl (Figure 6b).

### 3.3.2 | hiPSC-ECs attenuate demyelination

Observed at demyelinating stage (6 dpl), hiPSC-EC significantly reduced the loss of myelin component in CC lesion after 4 days transplantation, as shown by a smaller area of the lesion marked by Fluoro-Myelin staining and immunohistochemistry with antibody against MOG (0.145 mm² LPC vs. 0.08 mm² LPC+ hiPSC-EC, $p < .05$, Figure 7a). These data indicate that hiPSC-ECs protect myelin from LPC induced demyelination when introduced at early stage of injury.

### 3.3.3 | hiPSC-EC transplantation increases OPC repopulation

Comparing with the controls, there was a marked increase in the density of oligodendrocyte lineage cells in the lesion area after hiPSC-EC

transplantation at both 6 dpl (SOX10+, 60.21 cells/mm² control vs. 90.09 cells/mm² hiPSC-EC, $p < .05$. Figure 8a,c) and 11 dpl (GFP+, 53.14 cells/mm² control vs. 127.10 cells/mm² hiPSC-EC, $p < .05$. Figure 6c). The GFP+ cells in the lesion area appeared having brighter GFP labelling and enlarged cell bodies (Figure 6c), representing a character of injury-activated OPCs or newly formed oligodendrocytes (Crawford et al., 2013). There was a significantly increased percentage of Ki67+ in total lineage cells in the lesion area with hiPSC-EC transplantation at 6 dpl (Ki67+ SOX10+/SOX10+, 3.67% control vs. 7.87% hiPSC-EC, $p < .05$. Figure 8a,c) but not 11 dpl (Ki67+ GFP+/GFP+, 11.14% control vs. 8.74% hiPSC-EC, $p > .05$. Figure 8b,d). However, at 11 dpl the density of Ki67+ GFP+ cells were still significantly higher in hiPSC-EC treated lesions (5.33 cells/mm² control vs. 9.85 cells/mm² hiPSC-EC, $p < .05$. Figure 8b,d). The increased density of proliferating cells in oligodendrocyte lineage cells indicates that the presence of exogenous hiPSC-ECs from early stage after demyelination promotes OPC proliferation and increases OPC repopulation, these corroborates the *in vitro* effects on OPC proliferation and migration.

To assess how the recruited OPCs processed to oligodendrocytes, we labeled these GFP+ cells with antibody against APC (CC-1), a marker for the differentiated OPCs, at 11 dpl. Indeed, the cell density of APC+ GFP+ oligodendrocytes in the hiPSC-EC treated lesions was much higher than that in the controls (39.85/mm² control vs. 85.9/mm² hiPSC-EC, $p < .05$. Figure 8e,g). However, the percentage of the APC+ GFP+ cells relative to total GFP+ cells was comparable in both groups (80.33% control vs. 75.41% hiPSC-EC, $p > .05$. Figure 8e,g). The increased absolute oligodendrocyte density in lesion corroborates the *in vitro* effects of hiPSC-EC on promoting OPC differentiation. It also indicates that the promoted OPC repopulation leads to increased number of activated progenitors primed for differentiation.

To determine whether hiPSC-EC transplantation can directly affect the survival of OPCs and oligodendrocytes *in vivo*, we performed TUNEL assay to assess the cell death in GFP+ cells in the

lesions at 11 dpl. Compared with the controls, the proportion of the TUNEL+ GFP+ cells in total GFP+ cells were significantly reduced in the hiPSC-EC transplanted lesions (12.51% control vs. 5.12% hiPSC-EC, $p < .05$. Figure 8f,h). This implies that the increased amount of OPCs or/and oligodendrocytes in the CC lesions is also attributable to their increased survival.
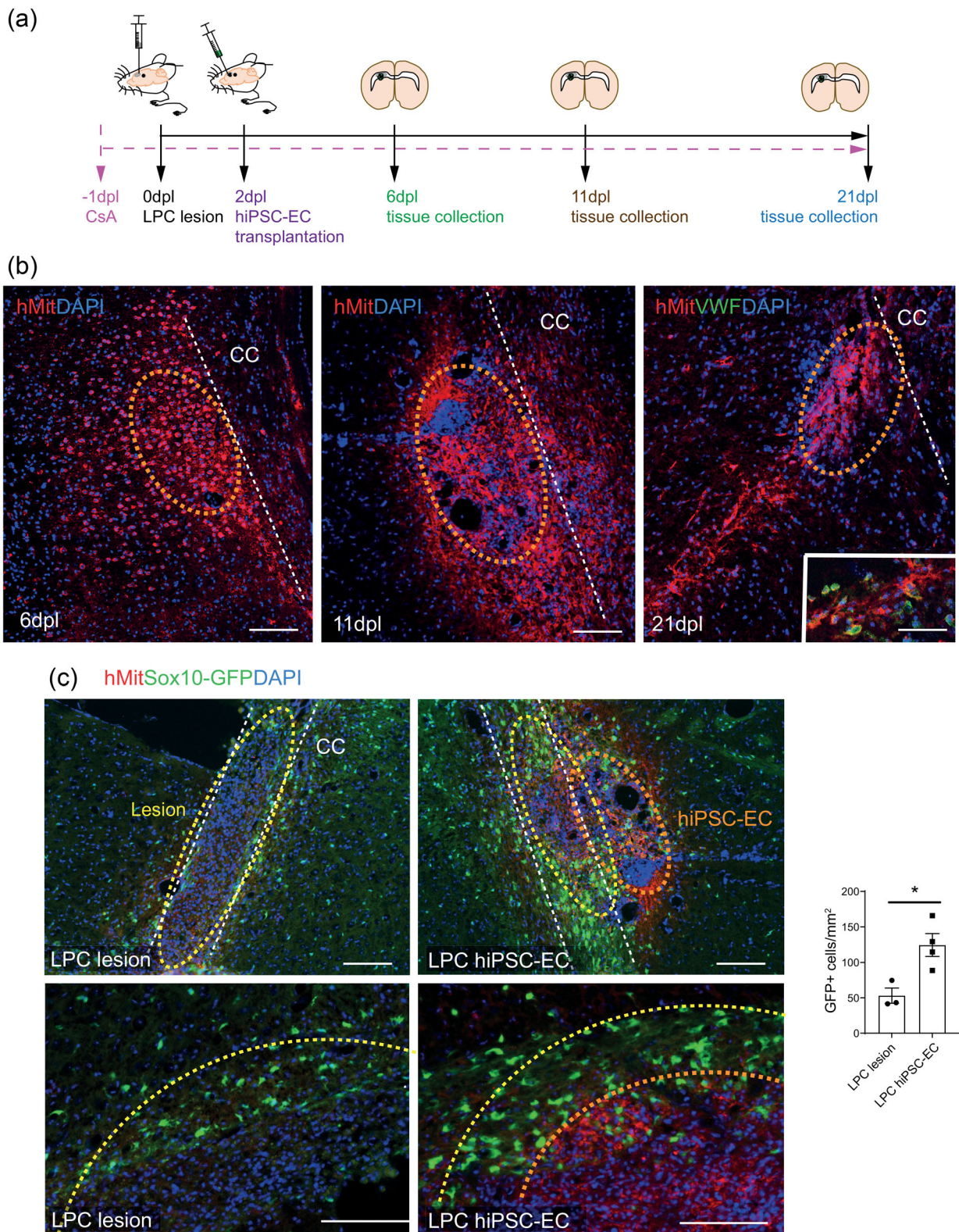


**FIGURE 6** Legend on next page.

### 3.3.4 | hiPSC-EC transplantation increases activation of mTORC1 pathway in oligodendrocyte lineage cells during remyelination

We further verified the involvement of mTORC1 activation in oligo-dendrocyte lineage progression following hiPSC-EC exposure *in vivo* by assessing pS6 level using immunohistochemistry at 11 dpl. Consistent with the *in vitro* observation, the intensity of pS6 labeling in GFP+ cells in the lesion area was significantly higher with the presence of transplanted iPSC-ECs than that in controls (65.86 control vs. 118.66 hiPSC-EC, Fiji Intensity, *p* < .01. Figure 8i,j). There was also an increased percentage of pS6+ GPF+ cells in total GFP+ cells in hiPSC-EC group (16.34% control vs. 27.83% hiPSC-EC, *p* < .05. Figure 8j). These observations confirmed that the transplanted hiPSC-ECs enhanced the activation of mTORC1 pathway at this stage of the lineage progression during remyelination. In the contralateral un-lesioned CC, there was no detectable immunolabeling of pS6 in GFP+ oligodendrocyte lineage cells in either control and hiPSC-EC group (Figure 8i,j), further indicating that the mTORC1 activation is an integral part of the activation and lineage progression of quiescent OPC in response to remyelination, but less so for myelin maintenance.

### 3.3.5 | hiPSC-EC transplantation improves remyelination

To examine the effect of hiPSC-EC transplantation on remyelination, we labeled the CC lesion area by immunohistochemistry for MBP, also a marker for myelin sheaths, at 11 dpl. The LPC-induced demyelin-ation caused a lower MBP labeling level than that in the un-lesioned area, while after hiPSC-EC transplantation, the lesions exhibited a higher intensity of MBP labeling (51.20 non-lesion vs. 7.34 LPC lesion vs. 23.35 LPC + hiPSC-EC, Fiji Intensity, *p* < .05. Figure 7c,d), together with evident morphology of myelinated fibers (Figure 7c). SOX10-GFP also labeled out myelin component, which showed a sim-ilar increased remyelination in hiPSC-EC group together with a higher population of GFP+ cells (Figures 6c,d and 7c). This data indicates that along with myelin protection at early stage, there was an improved remyelination following demyelination.

To assess the remyelination efficiency, we observed the myelin structure by EM at the late stage of remyelination (21 dpl). Although most axons had got remyelinated with thin myelin sheaths in control group, hiPSC-EC transplantation significantly increased the thickness of the newly formed myelin sheaths, as shown with a smaller *g*-ratio (0.91 control vs. 0.87 hiPSC-EC, *p* = 8.9−E06, Figure 7e−g). All these data indicate that hiPSC-ECs promote remyelination.

### 3.4 | hiPSC-ECs suppress neuroinflammation and promote microglial M2 polarization

Microglial phenotypes have differential regulatory functions on remyelination, and a predominant pro-regenerative response of microglia/macrophage (M2 phenotype) is required for efficient myelin repair after damage (Miron et al., 2013). To assess the effects of the hiPSC-EC on activation of microglia/macrophages, we first tested rat primary microglia in their responses to pro- and anti-inflammatory fac-tors. We co-cultured the hiPSC-ECs with rat microglia in the presence of pro-inflammatory factors TNFα or anti-inflammatory factor IL-4. Our data showed that after exposure to TNFα, hiPSC-ECs reduced endogenous TNFα expression in microglia (163.31 TNFα vs. 106.72 TNFα+hiPSC-EC, Fiji Intensity, *p* < .05, Figure 9a,b), while BDNF blocking antibody partially abolished this effect (106.72 TNFα+iPSC-EC vs. 145.20 TNFα+hiPSC-EC + aBDNF, Fiji Intensity, *p* < .01, Figure 9a,b). After exposure to IL-4, both IL-4 and hiPSC-EC increased Arg-1 expression individually in microglia (51.57 control vs. 134.17 IL-4, *p* < .01, vs. 96.67 hiPSC-EC, *p* < .05, Fiji Intensity, Figure 9c,d), while hiPSC-EC did not further enhance the expression by IL-4 (vs. 110.83 IL-4 + hiPSC-EC, *p* > .05, Figure 9c,d). BDNF blocking did not lead to any significant change in Arg-1 expression (Figure 9c,d). These *in vitro* data indicate that iPSC-ECs suppress M1 while promote M2 polarization in microglia, and BDNF is involved in attenuated M1 phenotype but not playing major role in promoting M2 phenotype by hiPSC-ECs.

We further assessed the inflammatory responses in CC lesions. At 6 dpl when demyelination was almost complete, there were IBA1+ activated microglia and macrophages densely aggregated within the CC lesions (Figure 9e). Transplantation of hiPSC-ECs dramatically

**FIGURE 6** Transplantation of hiPSC-ECs and its supportive effect on oligodendrocyte lineage cells in lesion area. (a) Schematic illustration of hiPSC-EC transplantation experiment. White matter demyelination was induced by focal injection of lysolecithin (LPC) in the corpus callosum (CC) at 0 day of post-lesion (dpl), hiPSC-ECs were injected into the lesion at 2–3 dpl, remyelination was assessed at 6 dpl, 11 dpl and 21 dpl. Cyclosporine (CsA) was added into drinking water from 1 day before (−1 dpl) demyelination lesioning till the end of experiment to all animals. (b) Representative images of hiPSC-EC grafts at 6, 11, and 21 dpl showing hiPSC-EC cell survival and migration. hiPSC-ECs were identified by immunolabeling using antibody against human mitochondria (hMit). The hiPSC-EC grafts are marked with orange dashed line. The insert shows the sustained EC property of transplanted hiPSC-ECs at 21 dpl with immunolabeling of EC marker vWF. Scale bar, 100 μm. (c) Representative images of the CC lesion area from the control and hiPSC-EC transplanted mice, which had SOX10-GFP reporter expression. CC is marked with white dashed line; demyelination lesion (determined by the aggregation of DAPI+ nuclei) is marked with yellow dashed line. The hiPSC-EC graft is marked with orange dashed line. The images show the overlapping of hiPSC-EC graft with the lesion and the aggregating of oligodendrocyte lineage cells (GFP+) in the lesion area. There is an increased GFP+ cell density in the presence of hiPSC-EC cells (red), and the size of the GFP+ cell bodies appear larger in the hiPSC-EC transplanted lesions. Scale bar, 200 μm. (d) Quantification shows an increased cell density of GFP+ OPCs and oligodendrocytes in the lesion area after hiPSC-EC transplantation. All data are presented as mean ± SE, *n* = 4, *p* < .05. Unpaired *t* test.
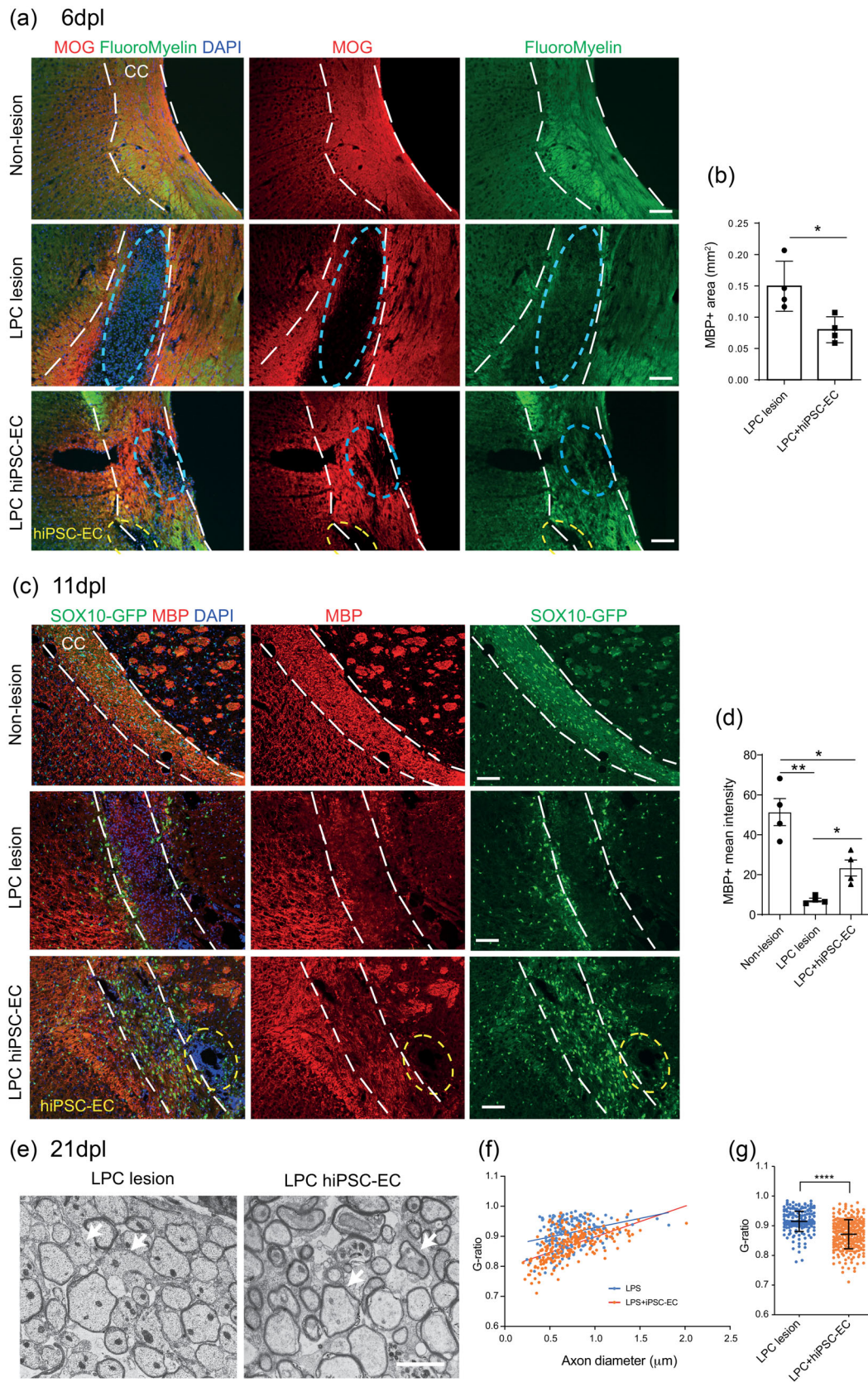
**FIGURE 7** Legend on next page.

reduced the IBA1+ cell distribution and IBA1+ area density (74.06% control vs. 42.05% hiPSC-EC, $p < .05$, Figure 9e,f). When double labeled with the M2 marker Arg-1, there was a significant increased proportion of Arg-1+ IBA1+ microglia/macrophages among total IBA1+ cells in hiPSC-EC group (9.72% control vs. 27.64% hiPSC-EC, $p < .05$, Figure 9e,f). These data indicate that hiPSC-ECs suppress inflammatory response and promote M2 phenotype at early remyelination stage. A higher proportion of M2 phenotype was also observed at the 11 dpl (Arg-1+ CD11b+/CD11b+, 52.5% control vs. 90.07% hiPSC-EC, $p < .05$, Figure S3), which could be conducive for OPC differentiation and maturation. These *in vivo* data further indicate that hiPSC-ECs suppress neuroinflammation and promote M2 polarization.

# 4 | DISCUSSION

Following CNS demyelinating injury, resting OPCs are first activated and recruited to the damaged area through proliferation and migration, then they engage with demyelinated axons and differentiate into mature oligodendrocytes to form new myelin. Therefore, sufficient activation, recruitment and OPC differentiation are the key initial events leading to successful remyelination (Franklin & ffrench-Constant, 2017; Zhao et al., 2015). The present study demonstrates that hiPSC-ECs facilitate oligodendrocyte lineage progression and transplantation benefits remyelination evidenced by higher OPC proliferation and differentiation/maturation. hiPSC-ECs also improve the survival of OPCs against pro-inflammatory cytokine *in vitro* and oligodendrocyte lineage cells *in vivo*, these might contribute to their myelin protection effect. Overall, our data indicate that hiPSC-ECs are beneficial to remyelination by protecting myelin and promoting repair.

OPC proliferation and differentiation are two inversely related cellular processes, differentiation usually coincides with proliferation arrest and exit from cell cycle, their enhancement by exposure to hiPSC-EC is likely a sequential event and mediated by activation of separate pathways. ECs secrete a cocktail of growth factors and cytokines (Arai & Lo, 2009; Grasman & Kaplan, 2017) which could exert different effects on oligodendrocyte lineage progression. Among them FGF and BDNF have been well known to support OPC survival and proliferation (Arai & Lo, 2009), whereas BDNF and TGFb individually facilitate OPC differentiation and oligodendrocyte maturation (Palazuelos et al., 2014; Xiao et al., 2010). Moreover, some of the factors may play their roles in a context dependent manner, facilitating OPC proliferation then differentiation by interacting with different factors. In addition, enhanced proliferation likely leads to subsequent increased differentiation. It has been reported that ECs improve OPC differentiation (Miyamoto et al., 2014) and iPSC-ECs promote remyelination in brain ischemic models (Xu et al., 2020, 2023). Furthermore, ECs and OPCs closely interact via both released factors and physical contact which regulate their functions mutually (Chavali et al., 2020; Manukjan et al., 2020). ECs change their properties during developmental and pathological conditions (Dejana et al., 2017), including the transition from acute to chronic inflammation (Miyamoto et al., 2014). It is conceivable that hiPSC-ECs switch their status with changing secretome following interactions with OPCs and oligodendrocytes both *in vitro* and *in vivo*. Future studies elucidating the dynamic secretome of ECs exposed to various stages of oligodendrocyte lineage progression will help pinpoint the underlying mechanisms how iPSC-ECs benefit myelin regeneration.

There are limited studies on whether and how ECs are directly beneficial to OPC differentiation; rather, it has been reported that rat primary ECs isolated from P14 inhibited OPC differentiation in co-culture system (Su et al., 2023). However, we have demonstrated here that hiPSC-ECs improved OPC differentiation after co-culture for a longer period, supported by a higher number of MPB+ OLs with more complex morphology. The discrepancy may arise from experimental settings such as species, age of ECs, and co-culture time (6 days vs. 2 days). The iPSC-ECs, with more pre-maturation characteristics (Bezenah et al., 2019; Jang et al., 2019), are expected to resemble more nascent, less specialized ECs which may have more potent effects on oligodendrocyte lineage progression compared to mature ECs. Although the proportion of the proliferating OPCs is higher in early stage (6 dpl) in lesion, the proportion of the differentiated oligodendrocytes across the whole lineage cells at later stage (11 dpl) was not reflecting the increase found *in vitro*. This might be due to the more complex regulatory process in the lesion environment, subtle changes in the rate of differentiation may have not been captured at selected time point in this study.

**FIGURE 7** hiPSC-EC transplantation attenuates myelin damage and enhances remyelination after LPC induced demyelination. (a) Representative images of MOG and FluoMyelin labelling in CC showing the myelin component in non-lesion, LPC lesion and in LPC plus hiPSC-EC groups at 6 dpl. CC is marked with white dashed line; the center of hiPSC-EC graft (overlapped with CC lesion) is marked by yellow dashed line. The lesion area is marked by blue dashed line. Scale bar, 200 μm. (b) Quantification of the lesion area in (a). (c) Representative images of MBP immunostaining in CC of SOX10-GFP mouse brains showing the myelin component in non-lesion, LPC lesion and LPC plus hiPSC-EC groups at 11 dpl. CC is marked with white dashed line; the center of hiPSC-EC graft (overlapped with CC lesion) is marked by yellow dashed line. Images show that the MBP labelling in lesion area is significantly reduced compared with unlesioned white matter, while it is partially recovered by hiPSC-EC transplantation. Scale bars, 200 μm. (d) Quantification of the MBP staining in (c), showing an increased intensity of MBP labelling in LPC plus hiPSC-EC group compared with LPC lesion group. All data are presented as mean ± SE, $n = 4$, *$p < .05$. One-way ANOVA with post hoc analysis. (e) Representative electron microscopic images of the lesion area at 21 dpl in control and hiPSC-EC groups showing an improved remyelination with hiPSC-EC transplantation. Note the thin myelin sheaths of remyelination (arrows) in control group and thicker myelin sheaths in hiPSC-EC group. Scale bar = 10 μm. (f) Quantification of (d), dots present g-ratio for each quantified axon. Data are mean ± SE. $n = 3$–5 animals, over 70 axons per animal. ****$p < .0001$, Unpaired $t$ test.
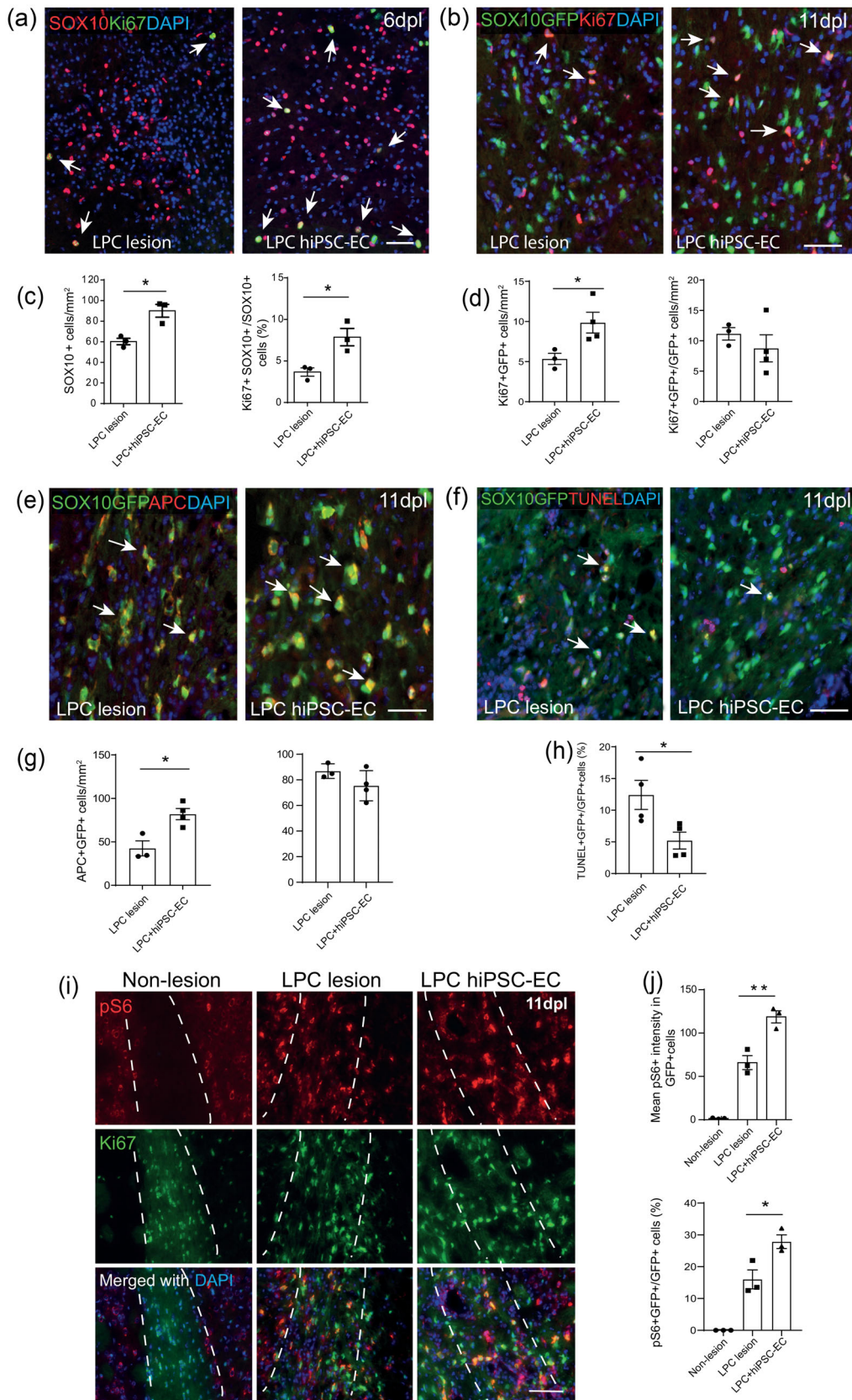
**FIGURE 8** Legend on next page.

BDNF is one of the major mediators for endothelium-oligodendrocyte interaction (Miyamoto et al., 2014). In this study, we show BDNF secreted from hiPSC-ECs mediated their pro-differentiation effects. It has been shown that BDNF promotes OPC differentiation into mature oligodendrocytes, which is mediated by Trk-B receptor and ERK pathway, BDNF also promotes myelin plasticity and repair (Fletcher et al., 2018; Xiao et al., 2010). Therefore, BDNF from hiPSC-ECs might contribute to promoting remyelination *in vivo*. BDNF is known to activate mTORC1 pathway which plays crucial roles in OPC differentiation during myelination and remyelination (Adams et al., 2021; Lebrun-Julien et al., 2014). Quiescent somatic stem cells in the intestinal epithelium of the fly and in the tracheal epithelium of mice exhibit transient activation of mTORC1 signaling during regeneration after injury (Haller et al., 2017). Although it is not clear whether a transient activation of mTORC1 signaling is also required for quiescent OPC activation, an increased mTORC1 activity in OPCs and newly differentiated oligodendrocytes with the presence of hiPSC-ECs *in vitro* and *in vivo* strongly suggests an important role of mTORC1 signaling pathway in hiPSC-EC mediated effects on oligodendrocyte lineage progression.

CNS injury induces neuroinflammation which involves the activation of microglia. At early stage, microglia/macrophages release pro-inflammatory cytokines and chemokines leading to further damage to the tissue. It has been reported that TNFα can induce oligodendrocyte and myelin pathology, but is required for OPC proliferation and remyelination (Arnett et al., 2001; Zahid et al., 2021). TNFα interferes with oligodendrocyte differentiation and causes their death, the effects are mediated by TNFR1 (Kim et al., 2011). In contrast, the activation of TNFR2 which is mainly expressed in OPCs promotes OPC proliferation and initiates pathways that drive oligodendrocytes into a reparative mode contributing to remyelination (Arnett et al., 2001; Madsen et al., 2016; Maier et al., 2013). We have shown in this study that hiPSC-ECs protect OPCs from TNFα-induced death with involvement of BDNF. This is consistent with a lower death rate in oligodendrocyte lineage cells in CC lesions. Therefore, the effect of hiPSC-ECs on remyelination might be contributed by their protective effects on OPCs against a proinflammatory environment, which is possibly associated with the secreted BDNF.

The oligodendrocyte lineage progression during remyelination is heavily modulated by neuroinflammation (Rawji et al., 2020). Microglia and macrophages manifest distinct M1 and M2 functional phenotypes at different stage of regeneration to modulate remyelination (Miron & Franklin, 2014). It has been reported that hiPSC-EC transplantation in CNS ischemia improves myelin repair via attenuated neuroinflammation in astrocytes, microglia/macrophages (Xu et al., 2020) and T cells (Xu et al., 2023). We have further shown in this study that hiPSC-ECs suppress inflammatory response while promote M2 polarization *in vitro* and *in vivo*. It has been reported that ECs provide an instructive niche for the differentiation and functional polarization of M2-like macrophages (He et al., 2012). Newly formed ECs reduce TNFα and IL-1β expression while increase CD206 (M2 marker) and IL-4R expression in macrophages which promotes functional recovery following spinal cord injury (Cohen et al., 2017). Indeed, ECs secret many factors such as IL-4, IL-13 and TGFb which are strong M2 stimulators. The reduced M1 phenotype and enhanced M2 phenotype by hiPSC-ECs observed in this study might contribute to both myelin protection and myelin repair. There is evidence that BDNF modulates marcrophage activation and promotes M2 polarization via TrkB signaling pathway (Covarrubias et al., 2016; Linton et al., 2019), and promotes M2 polarization of activated microglia after spinal cord injury (Ji et al., 2015). BDNF also suppresses LPS-induced microglial productions of pro-inflammatory cytokines (Wu et al., 2020). Our data show that BDNF is involved in hiPSC-EC attenuated M1 phenotype *in vitro*. Thus, the effects of iPSC-EC on oligodendrocyte lineage cells and neuroinflammation synergistically promote CNS remyelination.

Human iPSC technology is a breakthrough in regenerative medicine. iPSC derived OPCs or oligodendrocytes have been used to study myelin diseases (Chanoumidou et al., 2020). Comparing to OPCs, ECs can be derived faster from iPSCs with higher efficiency, although there are still challenges exiting (Williams & Wu, 2019). We have modified the EC induction method, which achieved a remarkable efficiency with a purity reaching 98%. Human iPSC-ECs have recently emerged as an attractive cell type for treating myocardial ischemia, peripheral vascular disease, and wound healing (Clayton et al., 2015, 2018). Our data show a therapeutic potential of iPSC-ECs in demyelinating diseases in the CNS.

**FIGURE 8** hiPSC-EC transplantation promotes oligodendrocyte lineage progression with increased mTORC1 activation. (a) Representative images of LPC-induced demyelinated area in CC in control and hiPSC-EC transplantation groups with Ki67 immunolabeling in SOX10 positive oligodendrocyte lineage cells at 6 dpl, or (b) in SOX10-GFP cells at 11 dpl (white arrows). (c) Quantification of (a) shows an increased cell density and proportion of the proliferating OPCs (Ki67+ SOX10+ cells), or (d) Ki67+ GFP+ cells. After hiPSC-EC transplantation, the proportion of Ki67+ cells in total SOX10+ cells are increased at 6 dpl while not changed at 11 dpl (in SOX10-GFP+ cells). (e) Representative images of the demyelinated area in CC in control and hiPSC-EC groups with APC immunolabeling in SOX10-GFP mice at 11 dpl, showing differentiated oligodendrocytes (APC+ GFP+, white arrows). (f) Representative images of cell death in GFP+ cells (TUNEL+ GFP+ cells, white arrows) in the demyelinated area in CC at 11 dpl. (g) Quantification of (e) shows an increased cell density of differentiated oligodendrocytes after hiPSC-EC transplantation. However, the proportion of APC+ cells in total GFP+ cells in transplantation group is comparable to controls. (h) Quantification of (f) shows a decreased percentage of TUNEL+GFP+ cells among GFP+ cells after hiPSC-EC transplantation. (i) Representative images of pS6 (Ser 240/244) immunolabeling in CC (white dashed lines) of SOX10-GFP mice at 11 dpl. In un-lesion area, the intensity of pS6 labelling is undetectable in GFP+ cells; it becomes stronger in demyelinated area, and the intensity is increased in GFP+ cells after iPSC-EC transplantation. (j) Quantification of (i) shows that both the intensity of pS6 labelling in GFP+ cells and the percentage of pS6+ GFP+ cells among GFP+ cells are significantly higher following hiPSC-EC transplantation. All data are presented as mean ± SE, $n = 4$, $*p < .05$, $**p < .01$. Unpaired $t$ test. Scale bars 50 μm.
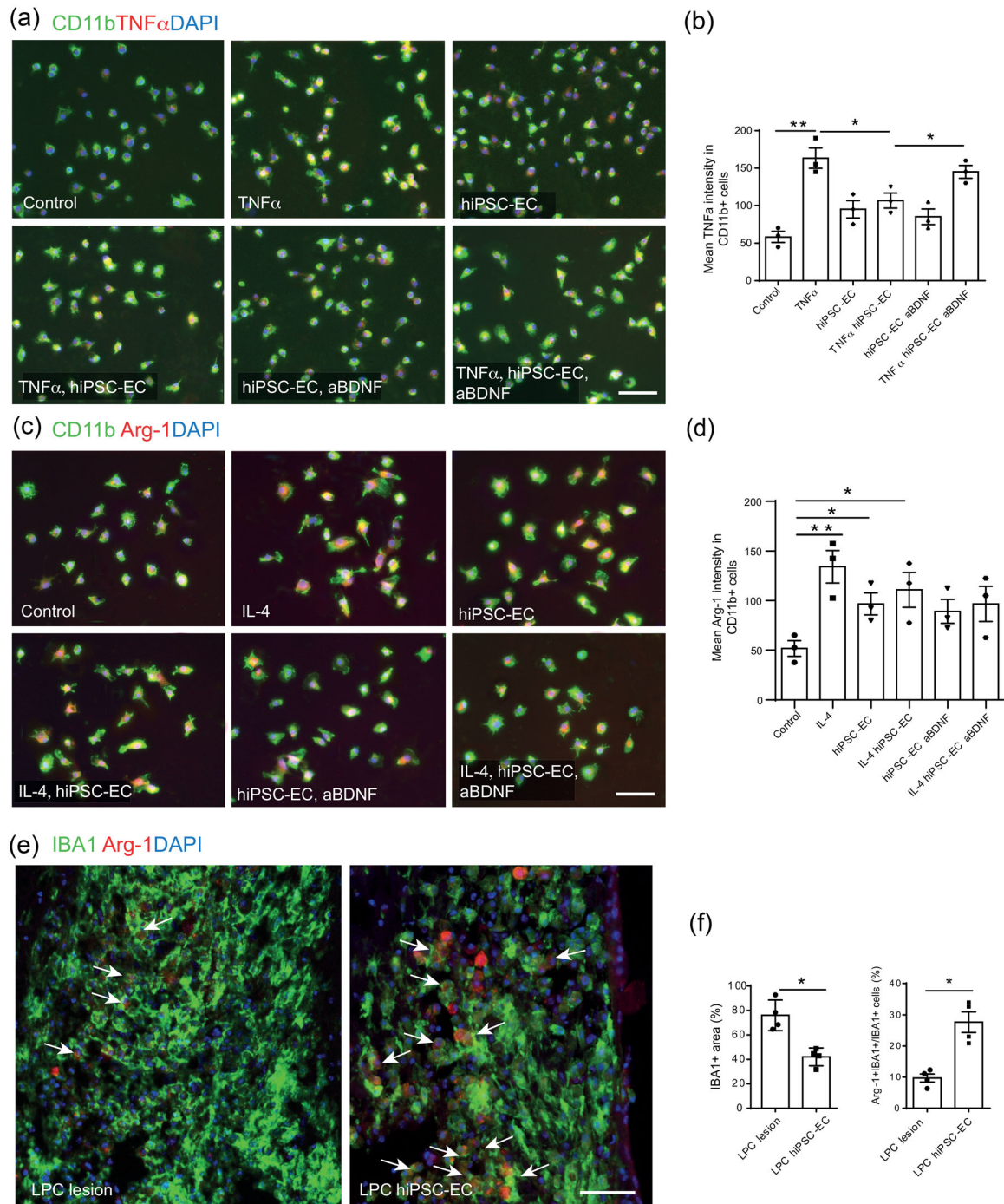
**FIGURE 9** Human iPSC-ECs suppress neuroinflammation while enhance M2 phenotype. (a) Representative images of rat microglia in culture treated with TNFα, hiPSC-ECs and anti-BDNF antibody. Microglia are immunolabeled by an antibody against CD11b, inflammatory reaction is marked by an antibody against TNFα. Scale bar: 50 μm. (b) Quantification of (a) shows the level of TNFα expression in microglia under different treatment, showing that hiPSC-ECs suppress inflammatory reaction and BDNF blocking partially reduces this effect. (c) Representative images of rat microglia in culture treated with IL-4, hiPSC-ECs and anti-BDNF antibody. Microglia were immunolabeled by an antibody against CD11b, M2 phenotype was immunolabeled by an antibody against Arg-1. (d) Quantification of (c) shows the level of Arg-1 expression in microglia under different treatment, revealing an increased Arg-1 expression in IL-4 and hiPSC-EC treatments individually, while BDNF blocking did not show significant change on hiPSC-EC effect. Scale bar: 40 μm. (e) Representative images of IBA1 immunostaining of microglia/macrophage in LPC induced lesions and in hiPSC-EC transplanted lesions in CC at 6 dpl, showing a decreased microglial/macrophage accumulation and an increased expression of Arg-1 in these cells in the lesions with hiPSC-EC transplantation. Scale bars, 100 μm. (f) Quantification of (e) shows a decreased area density of IBA1+ structures and a higher proportion of Arg-1+ microglia/macrophages in total IBA1+ cells, indicating an increased M2 phenotype among reactive microglia/macrophage in hiPSC-EC group. All data are presented as mean ± SE, $n = 4$, *$p < .05$, **$p < .01$. Unpaired $t$ test. In (b) and (d), one-way ANOVA with post hoc analysis.

# 5 | CONCLUSION

We have demonstrated that hiPSC-ECs enhance myelin repair after myelin injury in CNS. The effects are exerted by directly promoting oligodendrocyte lineage progression and indirectly modulating neuroinflammation. The hiPSC-EC secreted factors including BDNF contribute to these beneficial effects which involves mTORC1 signaling pathway. Further studies are required to determine the key signaling molecules. Human iPSCs provide a sustainable source of human cells for clinical use which overcomes numerous ethical and practical issues in research and clinical practice. Therefore, hiPSC-ECs hold the potential to be a source of cell therapy for a wide range of the diseases and injuries associated with myelin damage.

## AUTHOR CONTRIBUTIONS

Dan Ma and Chao Zhao conceptualized and designed the study. Dan Ma, Chao Zhao and Huiyuan Zhang wrote the manuscript. Dan Ma, Huiyuan Zhang, Hao Xu, Le Yin, Lida Wu, Rahul Shaji, Fatema Rezai, Ayesha Mulla, Sukhteerath Kaur and Chao Zhao performed experiments and analyzed results. Dan Ma, Chao Zhao, Shengjiang Tan and Yuchun Gu supervised and coordinated the study. Zhiguo Chen, Boris Kysela and Yilong Wang contributed to the discussion. All authors contributed to the article and approved the submitted version.

## CONFLICT OF INTEREST STATEMENT

The authors declare no potential conflict of interest.

## DATA AVAILABILITY STATEMENT

The original data presented in the study are included in the article material, further inquiries can be directed to the corresponding authors.

## ORCID

*Dan Ma* 🔵 https://orcid.org/0000-0001-8628-8954

## REFERENCES

Abbott, N. J., Rönnbäck, L., & Hansson, E. (2006). Astrocyte–endothelial interactions at the blood–brain barrier. *Nature Reviews Neuroscience*, 7, 41–53.

Adams, K. L., Dahl, K. D., Gallo, V., & Macklin, W. B. (2021). Intrinsic and extrinsic regulators of oligodendrocyte progenitor proliferation and differentiation. *Seminars in Cell & Developmental Biology*, 116, 16–24.

Arai, K., & Lo, E. H. (2009). An oligovascular niche: Cerebral endothelial cells promote the survival and proliferation of oligodendrocyte precursor cells. *The Journal of Neuroscience*, 29, 4351–4355.

Arnett, H. A., Mason, J., Marino, M., Suzuki, K., Matsushima, G. K., & Ting, J. P. (2001). TNF alpha promotes proliferation of oligodendrocyte progenitors and remyelination. *Nature Neuroscience*, 4, 1116–1122.

Attoff, K., Johansson, Y., CEDIEL-Ulloa, A., Lundqvist, J., Gupta, R., Caiment, F., Gliga, A., & Forsby, A. (2020). Acrylamide alters CREB and retinoic acid signalling pathways during differentiation of the human neuroblastoma SH-SY5Y cell line. *Scientific Reports*, 10, 1–15.

Baaklini, C. S., Rawji, K. S., Duncan, G. J., Ho, M. F., & Plemel, J. R. (2019). Central nervous system remyelination: Roles of glia and innate immune cells. *Frontiers in Molecular Neuroscience*, 12, 225.

Barateiro, A., Brites, D., & Fernandes, A. (2016). Oligodendrocyte development and myelination in neurodevelopment: Molecular mechanisms in health and disease. *Current Pharmaceutical Design*, 22, 656–679.

Bezenah, J. R., Rioja, A. Y., Juliar, B., Friend, N., & Putnam, A. J. (2019). Assessing the ability of human endothelial cells derived from induced-pluripotent stem cells to form functional microvasculature in vivo. *Biotechnology and Bioengineering*, 116, 415–426.

Bonora, M., DE Marchi, E., Patergnani, S., Suski, J. M., Celsi, F., Bononi, A., Giorgi, C., Marchi, S., Rimessi, A., Duszyński, J., Pozzan, T., Wieckowski, M. R., & Pinton, P. (2014). Tumor necrosis factor-α impairs oligodendroglial differentiation through a mitochondria-dependent process. *Cell Death and Differentiation*, 21, 1198–1208.

Chanoumidou, K., Mozafari, S., Baron-Van Evercooren, A., & Kuhlmann, T. (2020). Stem cell derived oligodendrocytes to study myelin diseases. *Glia*, 68, 705–720.

Chavali, M., ULLOA-Navas, M. J., Perez-Borreda, P., GARCIA-Verdugo, J. M., Mcquillen, P. S., Huang, E. J., & Rowitch, D. H. (2020). Wnt-dependent Oligodendroglial-endothelial interactions regulate white matter vascularization and attenuate injury. *Neuron*, 108(1130–1145), e5.

Chen, Y., Balasubramaniyan, V., Peng, J., Hurlock, E. C., Tallquist, M., Li, J., & Lu, Q. R. (2007). Isolation and culture of rat and mouse oligodendrocyte precursor cells. *Nature Protocols*, 2, 1044–1051.

Clayton, Z., Sadeghipour, S., & Patel, S. (2015). Generating induced pluripotent stem cell derived endothelial cells and induced endothelial cells for cardiovascular disease modelling and therapeutic angiogenesis. *International Journal of Cardiology*, 197, 116–122.

Clayton, Z. E., Tan, R. P., Miravet, M. M., Lennartsson, K., Cooke, J. P., Bursill, C. A., Wise, S. G., & Patel, S. (2018). Induced pluripotent stem cell-derived endothelial cells promote angiogenesis and accelerate wound closure in a murine excisional wound healing model. *Bioscience Reports*, 38, BSR20180563.

Cohen, M., Ben-Yehuda, H., Porat, Z., Raposo, C., Gordon, S., & Schwartz, M. (2017). Newly formed endothelial cells regulate myeloid cell activity following spinal cord injury via expression of CD200 ligand. *The Journal of Neuroscience*, 37, 972–985.

Covarrubias, A. J., Aksoylar, H. I., Yu, J., Snyder, N. W., Worth, A. J., Iyer, S. S., Wang, J., BEN-Sahra, I., Byles, V., POLYNNE-Stapornkul, T., Espinosa, E. C., Lamming, D., Manning, B. D., Zhang, Y., Blair, I. A., & Horng, T. (2016). Akt-mTORC1 signaling regulates Acly to integrate metabolic input to control of macrophage activation. *eLife*, 5, e11612.

Crawford, A., Chambers, C., & Franklin, R. (2013). Remyelination: The true regeneration of the central nervous system. *Journal of Comparative Pathology*, 149, 242–254.

Crawford, A. H., Tripathi, R. B., Richardson, W. D., & Franklin, R. J. (2016). Developmental origin of oligodendrocyte lineage cells determines response to demyelination and susceptibility to age-associated functional decline. *Cell Reports*, 15, 761–773.

Dejana, E., Hirschi, K. K., & Simons, M. (2017). The molecular basis of endothelial cell plasticity. *Nature Communications*, 8, 14361.

Fletcher, J. L., Murray, S. S., & Xiao, J. (2018). Brain-derived neurotrophic factor in central nervous system myelination: A new mechanism to promote myelin plasticity and repair. *International Journal of Molecular Sciences*, 19, 4131.

Franklin, R. J. M., & ffrench-Constant, C. (2017). Regenerating CNS myelin—From mechanisms to experimental medicines. *Nature Reviews. Neuroscience*, 18, 753–769.

Franklin, R. J. M., & Simons, M. (2022). CNS remyelination and inflammation: From basic mechanisms to therapeutic opportunities. *Neuron*, 110, 3549–3565.

Grasman, J. M., & Kaplan, D. L. (2017). Human endothelial cells secrete neurotropic factors to direct axonal growth of peripheral nerves. *Scientific Reports*, 7, 4092.

Haller, S., Kapuria, S., Riley, R. R., O'leary, M. N., Schreiber, K. H., Andersen, J. K., Melov, S., Que, J., Rando, T. A., Rock, J., Kennedy, B. K., Rodgers, J. T., & Jasper, H. (2017). mTORC1 activation during repeated regeneration impairs somatic stem cell maintenance. *Cell Stem Cell*, 21(806–818), e5.

He, H., Xu, J., Warren, C. M., Duan, D., Li, X., Wu, L., & IRUELA-Arispe, M. L. (2012). Endothelial cells provide an instructive niche for the differentiation and functional polarization of M2-like macrophages. *Blood*, 120, 3152–3162.

Jang, S., Collin De L'hortet, A., & SOTO-Gutierrez, A. (2019). Induced pluripotent stem cell-derived endothelial cells: Overview, current advances, applications, and future directions. *The American Journal of Pathology*, 189, 502–512.

Ji, X. C., Dang, Y. Y., Gao, H. Y., Wang, Z. T., Gao, M., Yang, Y., Zhang, H. T., & Xu, R. X. (2015). Local injection of Lenti-BDNF at the lesion site promotes M2 macrophage polarization and inhibits inflammatory response after spinal cord injury in mice. *Cellular and Molecular Neurobiology*, 35, 881–890.

Kim, S., Steelman, A. J., Koito, H., & Li, J. (2011). Astrocytes promote TNF-mediated toxicity to oligodendrocyte precursors. *Journal of Neurochemistry*, 116, 53–66.

Lebrun-Julien, F., Bachmann, L., Norrmen, C., Trotzmuller, M., Kofeler, H., Ruegg, M. A., Hall, M. N., & Suter, U. (2014). Balanced mTORC1 activity in oligodendrocytes is required for accurate CNS myelination. *The Journal of Neuroscience*, 34, 8432–8448.

Lian, X., Zhang, J., Zhu, K., Kamp, T. J., & Palecek, S. P. (2013). Insulin inhibits cardiac mesoderm, not mesendoderm, formation during cardiac differentiation of human pluripotent stem cells and modulation of canonical Wnt signaling can rescue this inhibition. *Stem Cells*, 31, 447–457.

Linton, M. F., Moslehi, J. J., & Babaev, V. R. (2019). Akt signaling in macrophage polarization, survival, and atherosclerosis. *International Journal of Molecular Sciences*, 20, 2703.

Lyman, M., Lloyd, D. G., Ji, X., Vizcaychipi, M. P., & Ma, D. (2014). Neuroinflammation: The role and consequences. *Neuroscience Research*, 79, 1–12.

Madsen, P. M., Motti, D., Karmally, S., Szymkowski, D. E., Lambertsen, K. L., Bethea, J. R., & Brambilla, R. (2016). Oligodendroglial TNFR2 mediates membrane TNF-dependent repair in experimental autoimmune encephalomyelitis by promoting oligodendrocyte differentiation and remyelination. *The Journal of Neuroscience*, 36, 5128–5143.

Maier, O., Fischer, R., Agresti, C., & Pfizenmaier, K. (2013). TNF receptor 2 protects oligodendrocyte progenitor cells against oxidative stress. *Biochemical and Biophysical Research Communications*, 440, 336–341.

Manukjan, N., Ahmed, Z., Fulton, D., Blankesteijn, W. M., & Foulquier, S. (2020). A systematic review of WNT signaling in endothelial cell oligodendrocyte interactions: Potential relevance to cerebral small vessel disease. *Cells*, 9, 1545.

Mccarthy, K. D., & de Vellis, J. (1980). Preparation of separate astroglial and oligodendroglial cell cultures from rat cerebral tissue. *Journal of Cell Biology*, 85, 890–902.

Miron, V. E., Boyd, A., Zhao, J. W., Yuen, T. J., Ruckh, J. M., Shadrach, J. L., VAN Wijngaarden, P., Wagers, A. J., Williams, A., Franklin, R. J. M., & Ffrench-Constant, C. (2013). M2 microglia and macrophages drive oligodendrocyte differentiation during CNS remyelination. *Nature Neuroscience*, 16, 1211–1218.

Miron, V. E., & Franklin, R. J. (2014). Macrophages and CNS remyelination. *Journal of Neurochemistry*, 130, 165–171.

Miyamoto, N., Pham, L.-D. D., Seo, J. H., Kim, K.-W., Lo, E. H., & Arai, K. (2014). Crosstalk between cerebral endothelium and oligodendrocyte. *Cellular and Molecular Life Sciences*, 71, 1055–1066.

Nakagomi, N., Nakagomi, T., Kubo, S., NAKANO-Doi, A., Saino, O., Takata, M., Yoshikawa, H., Stern, D. M., Matsuyama, T., & Taguchi, A. (2009). Endothelial cells support survival, proliferation, and neuronal differentiation of transplanted adult ischemia-induced neural stem/progenitor cells after cerebral infarction. *Stem Cells*, 27, 2185–2195.

Neumann, B., Baror, R., Zhao, C., Segel, M., Dietmann, S., Rawji, K. S., Foerster, S., Mcclain, C. R., Chalut, K., & VAN Wijngaarden, P. (2019). Metformin restores CNS remyelination capacity by rejuvenating aged stem cells. *Cell Stem Cell*, 25(473–485), e8.

Niu, J., Tsai, H. H., Hoi, K. K., Huang, N., Yu, G., Kim, K., Baranzini, S. E., Xiao, L., Chan, J. R., & Fancy, S. P. J. (2019). Aberrant oligodendroglial-vascular interactions disrupt the blood-brain barrier, triggering CNS inflammation. *Nature Neuroscience*, 22, 709–718.

Palazuelos, J., Klingener, M., & Aguirre, A. (2014). TGFbeta signaling regulates the timing of CNS myelination by modulating oligodendrocyte progenitor cell cycle exit through SMAD3/4/FoxO1/Sp1. *The Journal of Neuroscience*, 34, 7917–7930.

Patsch, C., Challet-Meylan, L., Thoma, E. C., Urich, E., Heckel, T., O'sullivan, J. F., Grainger, S. J., Kapp, F. G., Sun, L., & Christensen, K. (2015). Generation of vascular endothelial and smooth muscle cells from human pluripotent stem cells. *Nature Cell Biology*, 17, 994–1003.

Rajani, R. M., Quick, S., Ruigrok, S. R., Graham, D., Harris, S. E., Verhaaren, B. F. J., Fornage, M., Seshadri, S., Atanur, S. S., Dominiczak, A. F., Smith, C., Wardlaw, J. M., & Williams, A. (2018). Reversal of endothelial dysfunction reduces white matter vulnerability in cerebral small vessel disease in rats. *Science Translational Medicine*, 10, eaam9507.

Rawji, K. S., Gonzalez Martinez, G. A., Sharma, A., & Franklin, R. J. M. (2020). The role of astrocytes in remyelination. *Trends in Neurosciences*, 43, 596–607.

Su, Y., Wang, X., Yang, Y., Chen, L., Xia, W., Hoi, K. K., Li, H., Wang, Q., Yu, G., Chen, X., Wang, S., Wang, Y., Xiao, L., Verkhratsky, A., Fancy, S. P. J., Yi, C., & Niu, J. (2023). Astrocyte endfoot formation controls the termination of oligodendrocyte precursor cell perivascular migration during development. *Neuron*, 111(190–201), e8.

Takahashi, K., Tanabe, K., Ohnuki, M., Narita, M., Ichisaka, T., Tomoda, K., & Yamanaka, S. (2007). Induction of pluripotent stem cells from adult human fibroblasts by defined factors. *Cell*, 131, 861–872.

Tsai, H. H., Niu, J., Munji, R., Davalos, D., Chang, J., Zhang, H., Tien, A. C., Kuo, C. J., Chan, J. R., Daneman, R., & Fancy, S. P. (2016). Oligodendrocyte precursors migrate along vasculature in the developing nervous system. *Science*, 351, 379–384.

Williams, I. M., & Wu, J. C. (2019). Generation of endothelial cells from human pluripotent stem cells: Methods, considerations, and applications. *Arteriosclerosis, Thrombosis, and Vascular Biology*, 39, 1317–1329.

Wu, S. Y., Pan, B. S., Tsai, S. F., Chiang, Y. T., Huang, B. M., Mo, F. E., & Kuo, Y. M. (2020). BDNF reverses aging-related microglial activation. *Journal of Neuroinflammation*, 17, 210.

Xiao, J., Wong, A. W., Willingham, M. M., VAN DEN Buuse, M., Kilpatrick, T. J., & Murray, S. S. (2010). Brain-derived neurotrophic factor promotes central nervous system myelination via a direct effect upon oligodendrocytes. *Neurosignals*, 18, 186–202.

Xu, B., Kurachi, M., Shimauchi-Ohtaki, H., Yoshimoto, Y., & Ishizaki, Y. (2020). Transplantation of iPS-derived vascular endothelial cells improves white matter ischemic damage. *Journal of Neurochemistry*, 153, 759–771.

Xu, B., Shimauchi-Ohtaki, H., Yoshimoto, Y., Sadakata, T., & Ishizaki, Y. (2023). Transplanted human iPSC-derived vascular endothelial cells promote functional recovery by recruitment of regulatory T cells to ischemic white matter in the brain. *Journal of Neuroinflammation*, 20, 11.

Zahid, M., Busmail, A., Penumetcha, S. S., Ahluwalia, S., Irfan, R., Khan, S. A., Rohit Reddy, S., Vasquez Lopez, M. E., & Mohammed, L. (2021). Tumor necrosis factor alpha blockade and multiple sclerosis: Exploring new avenues. *Cureus*, *13*, e18847.

Zhao, C., Fancy, S. P., ffrench-Constant, C., & Franklin, R. J. (2008). Osteopontin is extensively expressed by macrophages following CNS demyelination but has a redundant role in remyelination. *Neurobiology of Disease*, *31*, 209–217.

Zhao, C., Ma, D., Zawadzka, M., Fancy, S. P., ELIS-Williams, L., Bouvier, G., Stockley, J. H., DE Castro, G. M., Wang, B., & Jacobs, S. (2015). Sox2 sustains recruitment of oligodendrocyte progenitor cells following CNS demyelination and primes them for differentiation during remyelination. *Journal of Neuroscience*, *35*, 11482–11499.

## SUPPORTING INFORMATION

Additional supporting information can be found online in the Supporting Information section at the end of this article.